CERN-TH/97-328
hep-ph/9711337

Two Lectures on Heavy Quark Production in Hadronic Collisions [1]

Michelangelo L. MANGANO[2]
CERN, TH Division, Geneva, Switzerland
mlm@vxcern.cern.ch

Abstract

These lectures present a pedagogical introduction to the physics of heavy-flavour production in hadronic collisions. The first lecture gives the theoretical background, with a discussion of leading-order calculations and of the effects of next-to-leading-order corrections. The origin and implications of the large logarithmic corrections appearing at this order are presented in an elementary way. The second lecture provides a survey of current experimental data on charm and bottom production, and describes their comparison with theoretical predictions. We emphasize the role played by some non-perturbative effects in the determination of charm distributions, and study the theoretical systematic uncertainties which affect our predictions.

CERN-TH/97-328
February 12, 2014

[1] Presented at the International School of Physics "E. Fermi", Course CXXXVII, *Heavy flavour physics: a probe of Nature's grand design.*

[2] On leave of absence from INFN, Pisa, Italy

Heavy Quark Production in Hadronic Collisions

Michelangelo L. MANGANO[3]
CERN, TH Division, Geneva, Switzerland
mlm@vxcern.cern.ch

1 Introduction

Most of this wonderful School was devoted to illustrating the key role that heavy quarks occupy in helping physicists probe the structure of elementary particles and their interactions at the most fundamental level. Progress in understanding the main conceptual weaknesses of the Standard Model, such as the origin of the family structure or the origin of CP violation, might well come in the future from more accurate studies of bottom and top quark decays and interactions. The present set of lectures, will address instead less mind-boggling aspects of heavy-quark physics, namely the physics involved in their production. Nevertheless, as I hope these lectures will convince you of, there is more to learn from a theoretical study of heavy-quark production than just cross-sections and predictions for the numbers of b quarks to be expected at the LHC.

First of all, heavy-quark production provides a benchmark process for the study of perturbative QCD. This is because the heavy-quark mass m_Q defines the scale at which the strong-interaction coupling constant α_s is evaluated, and $m_Q \gg \Lambda_{QCD}$ implies that the production properties (at least at the inclusive level) should be calculable within perturbation theory (PT). The existence of heavy quarks with different masses ($m_c \simeq 1.5$ GeV, $m_b \simeq 5$ GeV, $m_t \simeq 175$ GeV), allows us to probe perturbative QCD in regions of different Q^2, where the relative impact of radiative corrections and non-perturbative (NP) effects are very different. For example, we know that NP effects are very important in turning a c-quark into a charmed hadron (say a D^+). Were we able to fully control the charm production within PT, we could then hope to disentangle the NP physics from the comparison of PT with data. I shall give some examples of this in the second part of these lectures.

The presence of a heavy quark in the final state is also a flag for very specific production mechanisms and selects specific classes of relevant higher-order corrections. This can be useful either as a probe of the nucleon structure, or as a test of our understanding of radiative corrections in QCD. For example:

- W+charm final states probe the strange content of the proton, since the leading production mechanism is $gs \to Wc$.
- Inclusive b production at high energy probes the gluon density of the proton, since the leading process is $gg \to b\bar{b}$.
- Associated production of W and heavy-quark pairs is sensitive to gluon-splitting processes, since the dominant production process is the production of a W and an off-shell gluon, which then *decays* to the heavy-quark pair: $q\bar{q}' \to Wg^* \to WQ\overline{Q}$.

[3]On leave of absence from INFN, Pisa, Italy

The top quark is the heaviest of the heavy quarks. The history of its discovery and a thorough review of its first measured properties have been nicely covered in Bellettini's lectures at this School. There you certainly learned how much of a theoretical input will be required in measuring important properties such as the top mass or the CKM couplings. The mass, for example, is measured in hadronic collisions by reconstructing multi-jet final states from the top decay. Statistical errors on $m_{\rm top}$ achievable at the LHC ($\ll 1$ GeV) are overwhelmed by the systematic uncertainties due to the description of top production and decay. In fact a theoretical knowledge of the structure of the top-decay jets and their origin is needed to accurately fit the measured mass distributions [1] and extract a mass parameter[4]. A similar need for theoretical input is required when extracting the top mass from the threshold behaviour in e^+e^- annihilations, one of the goals of future Next Linear Colliders [2]. The direct measurement of the CKM matrix element V_{tb} can be performed by detecting production of single quarks in hadron collisions, via the processes $q\bar{q}' \to W^* \to t\bar{b}$ and $gq \to t\bar{b}q'$ (where the exchange of a t-channel W is understood). In both these processes, in fact, the production rate is directly proportional to $|V_{tb}|^2$. Once more, accurate studies of the QCD aspect of the production dynamics need to be performed to make a meaningful measurement of $|V_{tb}|$ possible.

The study of b cross-sections at the Tevatron [3] is helping us to improve the reliability of our estimates of b rates at the LHC, where b's will be used to measure CP violation [4] and to probe possible b-meson rare decays, foreseen in several theories beyond the Standard Model, as reviewed in this School by Masiero. The expected total cross-sections will define overall rates, the kinematical distributions will determine triggering strategies and detector design.

Heavy quarks are also important signals of possible new physics, in addition to providing large backgrounds to searches for new physics:

Signals:	**Backgrounds:**
$H \to b\overline{b}$	$gg \to b\overline{b}$
$WH \to b\overline{b}$	$q\bar{q} \to Wb\overline{b}$
$\tilde{t} \to b\chi^+,\ c\chi^0,\ t\chi^0$	$p\bar{p} \to Wb\overline{b}jj, \quad \overline{t}t$
$b' \to \gamma b,\ Z^0 b$	$p\bar{p} \to b\overline{b}\gamma\gamma$
$\chi^+\chi_2^0 \to$ 3 lept's	$p\bar{p} \to t\overline{t}$
$\ldots$	$\ldots$

Understanding the characteristics of final states with b's (and b-jets) is fundamental in order to learn how to isolate signals from backgrounds.

As a final example of possible uses of heavy-quark production, let me mention the searches for quark-gluon plasma done in heavy-ion collisions. Among other probes, final states with J/ψ and, more generally, DY pairs, will be used to study the properties of matter at high density. Charm pairs will provide both signals ($c\bar{c} \to J/\psi$) and backgrounds ($c\bar{c} \to \mu^+\mu^-$). To make robust predictions on the properties of charm produced in high-energy nuclear collisions at future

[4]This is similar to what happens in the case of the Z mass measurement at LEP/SLC, where the Z mass is obtained from a fit to the Z lineshape. The lineshape is affected by higher-order QED corrections, mostly initial-state radiation. These need to be evaluated theoretically before the Z mass, which is a parameter in the fit, can be extracted from a comparison with the data.

machines (RHIC and LHC) it becomes important to test our understanding in simpler production environments, such as those provided by current fixed-target hadro- and photo-production experiments. Due to the smallness of the charm mass, significant NP corrections are expected. As mentioned earlier, this is therefore also an important place to study the interplay of perturbative and non-perturbative effects, as will be discussed in the second part of these lectures.

The structure of the lectures is as follows:

1. The theory of heavy-quark production:
   - leading order
   - total and differential cross-sections
   - NLO corrections
2. Phenomenology of heavy-quark production:
   - fixed-target charm production
   - interplay of perturbative and non-perturbative effects
   - bottom production at the Tevatron

2 Theory of heavy-quark production

In this Section I will present an elementary introduction to the theory of heavy-quark production in hadron-hadron collisions. Production of heavy quarks in e^+e^- collisions is to leading-order (LO) an electroweak process, and is therefore relatively straightforward to control. The complications of QCD arise only at the level of radiative corrections, and become relevant only when one is interested in high-precision studies (such as the measurement of R_b at LEP/SLC) or in particular aspects of the QCD dynamics (such as the study of fragmentation functions, to which we will return in the following). Photoproduction, which is of relevance for several fixed-target experiments and for the HERA collider, can be described by a sub-class of the processes appearing in hadronic collisions, so we will not consider it in detail here (although we will discuss its phenomenology in the second lecture). For a complete and more technical review of the theory of heavy-quark production, as well as for a precious list of references to the original papers, see for example Nason's work in ref. [5]. Additional details and phenomenological applications can be found in the excellent book by Ellis, Stirling and Webber [6].

2.1 Leading order

Two processes are responsible for heavy-quark hadro-production at the LO in perturbation theory:

$$q\bar{q} \to Q\overline{Q} \qquad \text{and} \qquad gg \to Q\overline{Q}\,. \tag{1}$$

The corresponding diagrams are shown if fig. 1. Few simple comments are in order:

- In $q\bar{q} \to Q\overline{Q}$, the $Q\overline{Q}$ pair is always in a colour-octet state. In $gg \to Q\overline{Q}$ both colour-singlet and octet are allowed.

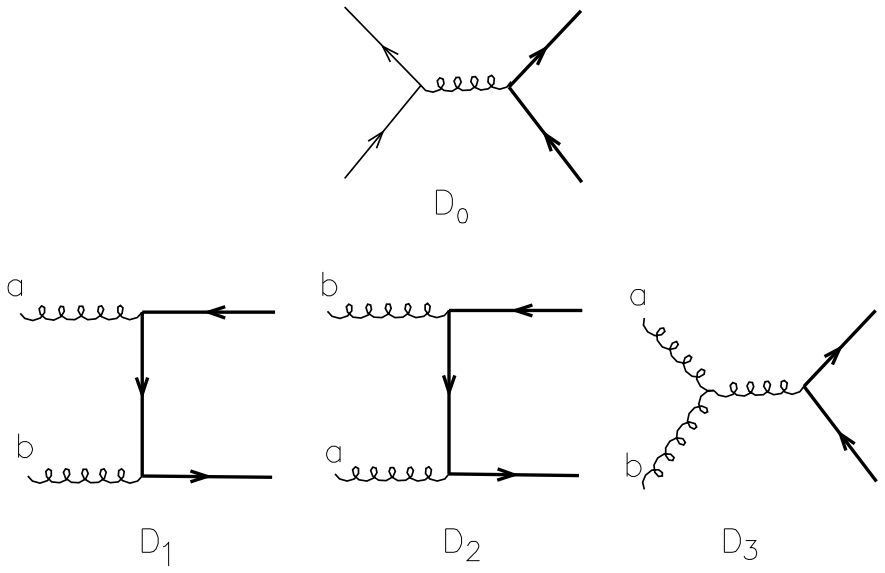

Figure 1: *Leading-order diagrams for heavy-quark pair production.*

- The process $q\bar{q} \to Q\overline{Q}$ is similar to $e^+e^- \to \mu^+\mu^-$. The only difference is an overall colour factor

$$\sum_a \lambda^a_{ij}\lambda^a_{kl} \equiv \frac{1}{2}(\delta_{il}\delta_{jk} - \frac{1}{N}\,\delta_{ij}\delta_{kl})\;, \tag{2}$$

  which when squared and summed over all possible initial and final colour states gives a factor $C_F = (N^2-1)/2N$ ($C_F = 4/3$ for $N = 3$).

- The total production cross-section for heavy quarks is finite. In fact no poles can develop in the intermediate propagators. This is obvious for the s-channel diagrams, since $s > 4m^2$. In the case of the t-channel gluon exchange (say in diagram D_1 of the figure), labeling the lower-line gluon and quark momenta as p_1 and Q, respectively, one obtains in the CM frame:

$$(p_1 - Q)^2 - m^2 = -2p_1 \cdot Q = -\frac{\hat{s}}{2}(1 - \beta\cos\theta) \tag{3}$$

  with β the heavy-quark velocity ($\beta \equiv \sqrt{1 - \frac{4m^2}{\hat{s}}}$) and θ the scattering angle. Therefore the propagator never vanishes:

$$2p_1 \cdot Q \geq \frac{\hat{s}}{2}(1-\beta) = \frac{\hat{s}}{2(1+\beta)}(1-\beta^2) = \frac{2m^2}{1+\beta} \geq m^2\;. \tag{4}$$

Therefore m^2 is the minimum virtuality exchanged in the t-channel, and the total cross-section is finite at LO in PT. This would not be the case for massless quarks. The minimum transverse momentum transferred in the t-channel sets the scale for the argument of the strong coupling constant α_s. Since this scale is of the order of the heavy-quark mass, and since this is (by definition of heavy quark) much large than Λ_{QCD}, perturbative calculations should be reliable. Once again, this could not be the case for light quarks: the *total* production cross-section for *up* or *down* quarks in not calculable in PT!

The evaluation of the matrix elements can be done using standard Feynman diagram techniques. The results are:

$$\frac{1}{g^4}\overline{\Sigma}\left|M(q\bar{q}\to Q\overline{Q})\right|^2 = \frac{V}{2N^2}(\tau_1^2+\tau_2^2+\frac{\rho}{2}) \quad (5)$$

$$\frac{1}{g^4}\overline{\Sigma}\left|M(gg\to Q\overline{Q})\right|^2 = \frac{1}{2VN}\left(\frac{V}{\tau_1\tau_2}-2N^2\right)\left(\tau_1^2+\tau_2^2+\rho-\frac{\rho^2}{4\tau_1\tau_2}\right) \quad (6)$$

where: $V=N^2-1$ is the dimension of the $SU(N)$ gauge group, i.e. the number of gluons, and

$$\tau_{1,2}=2\,\frac{p_{1,2}\cdot Q}{\hat{s}}=\frac{1\mp\beta\cos\Theta}{2}\,,\qquad \rho=\frac{4m^2}{\hat{s}},\qquad \hat{s}=(p_1+p_2)^2 \quad (7)$$

Exercise 1: show that in the limit $\tau_1\tau_2\to 0$ (which can be achieved at very high energy when $\beta\to 1$) the $gg\to Q\overline{Q}$ matrix element squared goes at most like $1/(\tau_1\tau_2)$, and not like $1/(\tau_1\tau_2)^2$, as the eq. (6) naively indicates.
Exercise 2: show that the term inside the first parenthesis of eq. (6) is always positive.

The total partonic cross-sections are obtained by integrating over the two-body phase space:

$$d\phi_{(2)}\equiv\frac{1}{2\hat{s}}\,\frac{d^2Q}{(2\pi)^3 2Q^0}\,\frac{d^3\overline{Q}}{(2\pi)^3 2\overline{Q}^0}\,(2\pi)^4\delta^4(P_{in}-P_{out}) = \frac{\pi}{2\hat{s}}\left(\frac{1}{4\pi}\right)^2\beta\;d(\cos\theta) \quad (8)$$

giving the following results:

$$\hat{\sigma}(q\bar{q}\to Q\overline{Q}) = \frac{\alpha_s^2}{m^2}\left(\frac{V}{N^2}\right)\frac{\pi\beta}{24}\rho(2+\rho)\overset{\hat{s}\to\infty}{\to}\frac{1}{\hat{s}} \quad (9)$$

$$\hat{\sigma}(gg\to Q\overline{Q}) = \frac{\alpha_s^2}{m^2}\left(\frac{1}{NV}\right)\frac{\pi\beta}{24}\rho\left[3\mathcal{L}(\beta)\left(\rho^2+2V(\rho+1)\right)\right.$$
$$\left.+2(V-2)(1+\rho)+\rho(6\rho-N^2)\right]\overset{\hat{s}\to\infty}{\to}\frac{1}{\hat{s}}\mathcal{L}(\beta) \quad (10)$$

where

$$\mathcal{L}(\beta)=\frac{1}{\beta}\log\left(\frac{1+\beta}{1-\beta}\right)-2 \quad (11)$$

Comments:

- At large $\hat{s}$ the $q\bar{q}$ rate vanishes more quickly.
- Notice that the threshold suppression in the $q\bar{q}\to Q\overline{Q}$ process goes like

$$\beta(2+\rho)=\sqrt{1-\rho}\,(2+\rho)\simeq 2(1-\frac{\rho}{2})(1+\frac{\rho}{2})=2(1-4\frac{m^4}{\hat{s}^2}) \quad (12)$$

  As a result threshold effects vanish very quickly as soon as $\hat{s}>4m^2$. This *suppressed suppression* is related to the spin-1/2 of quarks. For scalar particles (e.g., squarks) the phase-space suppression is stronger ($\sim\beta^3$).

This is important for top production, which for the measured value of the top mass is dominated at the Tevatron by $q\bar{q}$ annihilation close to the kinematic threshold. Including the reduction in rate due to the fewer degrees of freedom of a scalar particle relative to a spin-1/2 one, the squark cross-section turns out to be approximately 1/10 of that of a quark with the same mass, if the dominant production mechanism is $q\bar{q}$ annihilation.

Examples:

- The relative productions rates for heavy quarks of mass m_1 and m_2 behave, at high energy, like:

$$\frac{\hat{\sigma}(gg \to Q_1\overline{Q}_1)}{\hat{\sigma}(gg \to Q_2\overline{Q}_2)} \overset{s\to\infty}{\to} 1 - \frac{\log(m_1^2/m_2^2)}{\log(s/m_2^2)} \tag{13}$$

  For example,

$$\frac{\sigma(gg \to b\bar{b})}{\sigma(gg \to c\bar{c})} \sim 0.7 \qquad \text{at} \quad \sqrt{\hat{s}} = 100 \text{ GeV} \tag{14}$$

- For the $q\bar{q}$ process we have instead:

$$\frac{\hat{\sigma}(q\bar{q} \to Q_1\overline{Q}_1)}{\hat{\sigma}(q\bar{q} \to Q_2\overline{Q}_2)} \to 1 - O(m_1^4/\hat{s}^2) \tag{15}$$

  with

$$\frac{\sigma(q\bar{q} \to b\bar{b})}{\sigma(q\bar{q} \to c\bar{c})} \sim 0.99 \qquad \text{at} \quad \sqrt{\hat{s}} = 100 \text{ GeV} \tag{16}$$

In general, we are interested in *hadronic* rather than *partonic* rates. The obtain these we need to convolute the partonic cross-sections with the parton densities in the hadron. It is then useful to parametrize the final state in terms of the transverse momentum ($p_\perp$) and of the rapidities (y) of the produced quarks. The resulting phase-space, including the integration over the momentum fractions of the hadrons carried by the initial-state partons $x_{1,2}$, is then:

$$d\phi_{p\bar{p}} = \frac{1}{2\hat{s}}\, dx_1 dx_2 \frac{d^3Q}{(2\pi)^3 2q^0}\, \frac{d^3\overline{Q}}{(2\pi)^3 2\overline{Q}^0}\, (2\pi)^4\delta^4(P_{\text{in}} - P_{\text{out}}) \tag{17}$$

Use:

$$dx_1 dx_2\ \delta(E_{\text{in}} - E_{\text{out}})\delta(P^z_{\text{in}} - P^z_{\text{out}}) = \frac{1}{2E^2_{\text{beam}}} = \frac{2}{S_{\text{had}}} \tag{18}$$

$$\frac{dQ_z}{Q^0} = dy\ , \quad y = \frac{1}{2}\log\frac{Q^0 + Q^z}{Q^0 - Q^z} \quad (\to \eta = -\log(\tan\frac{\theta}{2}) \quad \text{for} \quad m = 0) \tag{19}$$

to get:

$$d\phi_{p\bar{p}} = \frac{\pi x_1 x_2}{\hat{s}^2}\left(\frac{1}{4\pi}\right)^2 dy d\bar{y} dp_T^2 \tag{20}$$

It is easy to rewrite $\hat{s}$ in terms of $y, \bar{y}$ and of the transverse mass $m_T^2 = p_\perp^2 + m^2$ using:

$$\begin{cases} Q_0 &= m_T\ \cosh y \\ Q_z &= m_T\ \sinh y \end{cases} . \tag{21}$$

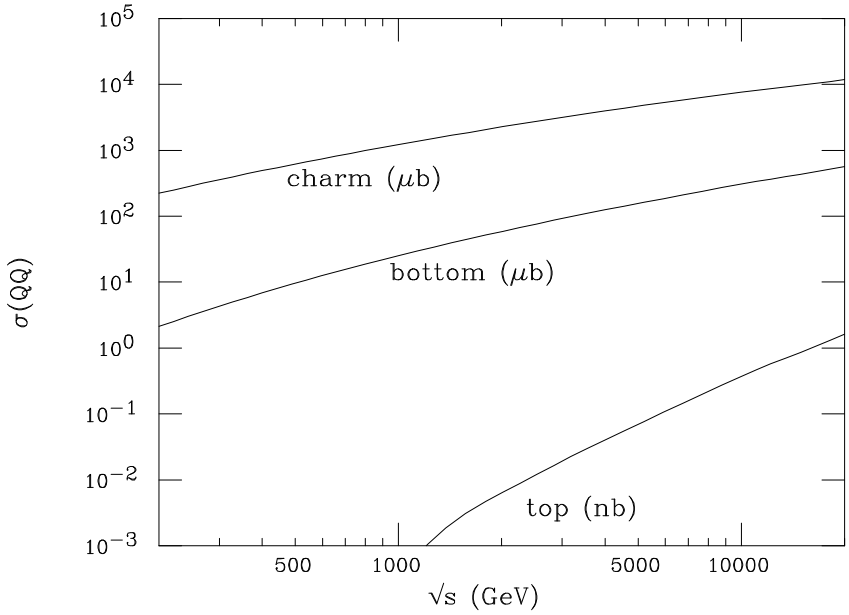

Figure 2: *Total production cross-sections for charm, bottom and top quark pairs, in $p\bar{p}$ collisions.*

This gives: $\hat{s} = 2m_T^2 \{1 + \cosh(y - \bar{y})\}$ and finally:

$$\frac{d\sigma}{dyd\bar{y}dp_T^2} = \frac{\pi}{4m_T^4} \frac{1}{[1 + \cosh(y - \bar{y})]^2} \frac{1}{(4\pi^2)} \times \sum_{i,j} x_1 f_i(x_1) x_2 f_j(x_2) \overline{\sum} |M(ij \to Q\overline{Q})|^2 \qquad (22)$$

For a fixed value of p_T (and therefore of m_T), the rate is heavily suppressed when $|y - \bar{y}|$ becomes large. Therefore Q and $\overline{Q}$ tend to be produced with the same rapidity. This has important consequences for the design of detectors aimed at collecting large numbers of $b\bar{b}$ pairs, as required to perform CP studies. In fact, it implies that once a detector has registered the b quark, there is a large probability that the $\bar{b}$ will be nearby in rapidity. This is fundamental for detectors covering the forward region only, since it shows that there is no need to build a backward spectrometer as well to efficiently collect the heavy-quark *pair*. The gain in acceptance for the pair would only be a factor of 2, and not 4 as naively expected in absence of such strong rapidity correlations!

2.2 Some results

We discuss here some simple applications of the cross-section formulae obtained in the previous section. They can be convoluted numerically with standard parametrizations of the parton densities inside the proton, to obtain hadronic cross-setions at different energies and for different quark masses. In fig. 2 I show the total production cross-sections in $p\bar{p}$ collisions, as a function of the hadronic center of mass energy $\sqrt{S}$, for charm, bottom and top quark pairs. Notice the different units used in the case of the top quark relative to those used for charm and bottom! Top cross sections are suppressed by several orders of magnitude even at the highest energies reachable in the foreseeable future. When the *partonic* CM energy grows, however, the suppression due to the large mass becomes less and less important, as discussed in the previous section. This can

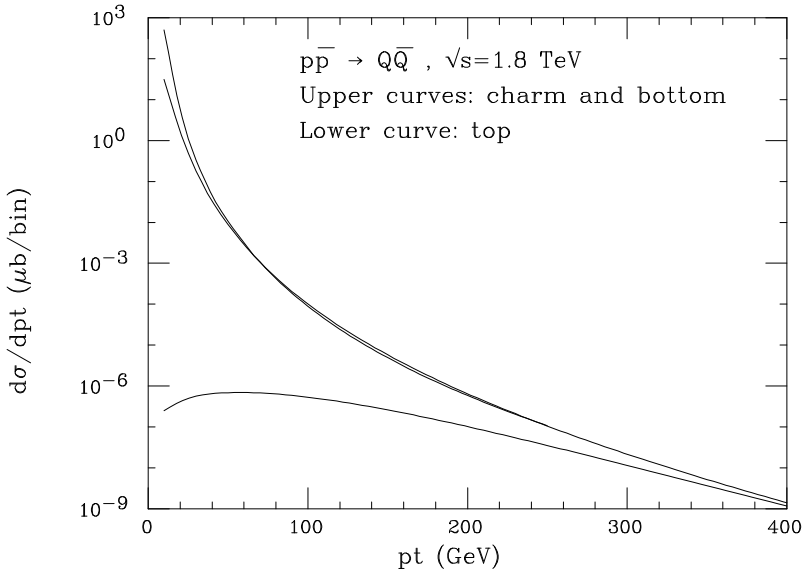

Figure 3: *Inclusive p_T distributions for charm, bottom and top quarks pairs, in $p\bar{p}$ collisions at $\sqrt{S} = 1.8$ TeV.*

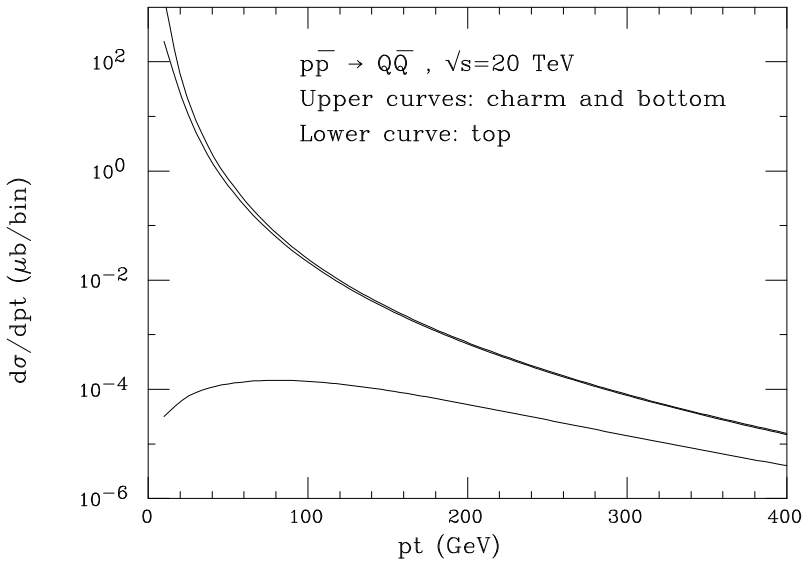

Figure 4: *Inclusive p_T distributions for charm, bottom and top quarks pairs, in $p\bar{p}$ collisions at $\sqrt{S} = 20$ TeV.*

be seen in fig. 3, which shows the transverse momentum distributions at $\sqrt{S} = 1.8$ TeV. Notice that the charm and bottom rates become almost equal as soon as $p_T \gtrsim 40$ GeV (which means $\sqrt{\hat{s}} \gtrsim 80$ GeV). In the case of the top, we need to go out to $p_T > 400$ GeV. It is instructive to see how this picture changes at higher hadronic energies. This is shown in fig. 4 for $\sqrt{S} = 20$ TeV. Notice that at $p_T = 400$ GeV there is still a large difference between the c, b rates and the top rate. This is because, contrary to the case of 1.8 TeV, at the LHC the production rate is dominated by

gg annihilation. As we showed earlier, the mass effects vanish more slowly for gg processes than for the $q\bar{q}$ annihilation process. More details on the comparison of the predicted production rates with the available experimental data will be given in the second lecture. For the time being, we shall move on to the discussion of the corrections beyond the Born level.

2.3 Next-to-leading order corrections

Next-to-leading-order (NLO) corrections come from two sources of $O(\alpha_s^3)$ diagrams:

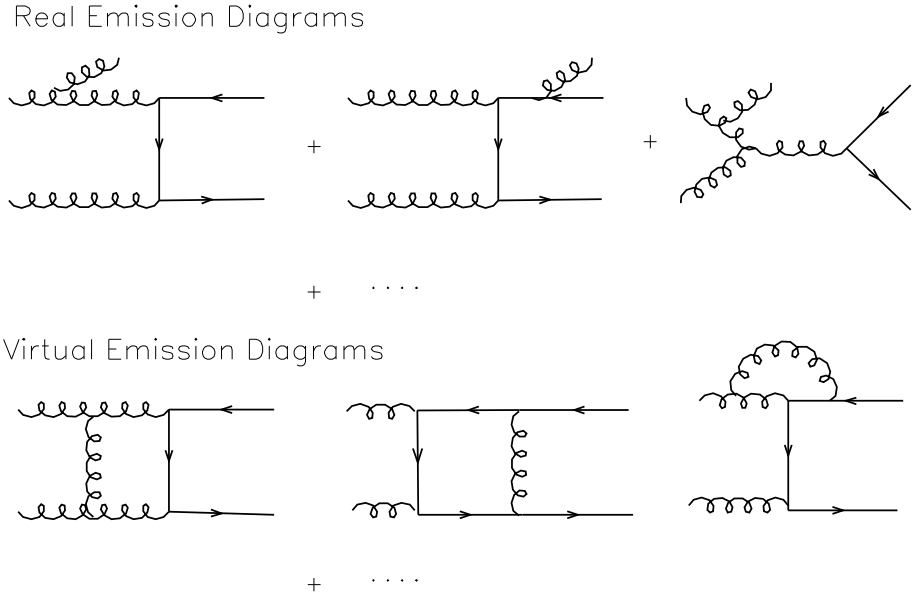

In the first case, the corrections come from the square of the real emission matrix elements. In the second case, from the interference of the virtual matrix elements (of $O(g^4)$) with the Born level ones (of $O(g^2)$). Ultraviolet divergences in the virtual diagrams are removed by the renormalization process. Infrared and collinear divergences which appear both in the virtual diagrams and in the integration over the emitted parton in the real-emission processes cancel each other, or are absorbed in the initial-state parton densities. The complete calculations of NLO corrections to the production of heavy-quark pairs in hadro- and in photo-production were done in ref. [7, 8] (total hadroproduction cross-sections), ref. [9, 10] (one-particle inclusive distributions in hadroproduction), ref. [11, 12] (total and one-particle inclusive distributions in photoproduction), ref. [13] (two-particle inclusive distributions in hadroproduction) and ref. [14] (two-particle inclusive distributions in photoproduction). The explicit results are too complicated for me to reproduce them here. So I will limit myself to a qualitative discussion only.

NLO corrections should improve our knowledge of the production cross-section. In particular, uncertainties related to the renormalization ($\mu_{\rm R}$) and factorization ($\mu_{\rm F}$) scale dependence should be reduced[5]. There is evidence however that the NLO is not sufficient to get accurate estimates, since a large scale dependence is still present. This is shown is fig. 5, which shows the scale dependence of the inclusive p_T distribution of b quarks at the Tevatron. Large scale dependence is a symptom of large NNLO corrections A full NNLO calculation goes beyond our ability. So, we are stuck.

[5]The renormalization scale $\mu_{\rm R}$ is the energy scale used in the evaluation of α_s. The factorization scale $\mu_{\rm F}$ is the scale used in the evolution of the parton densities.

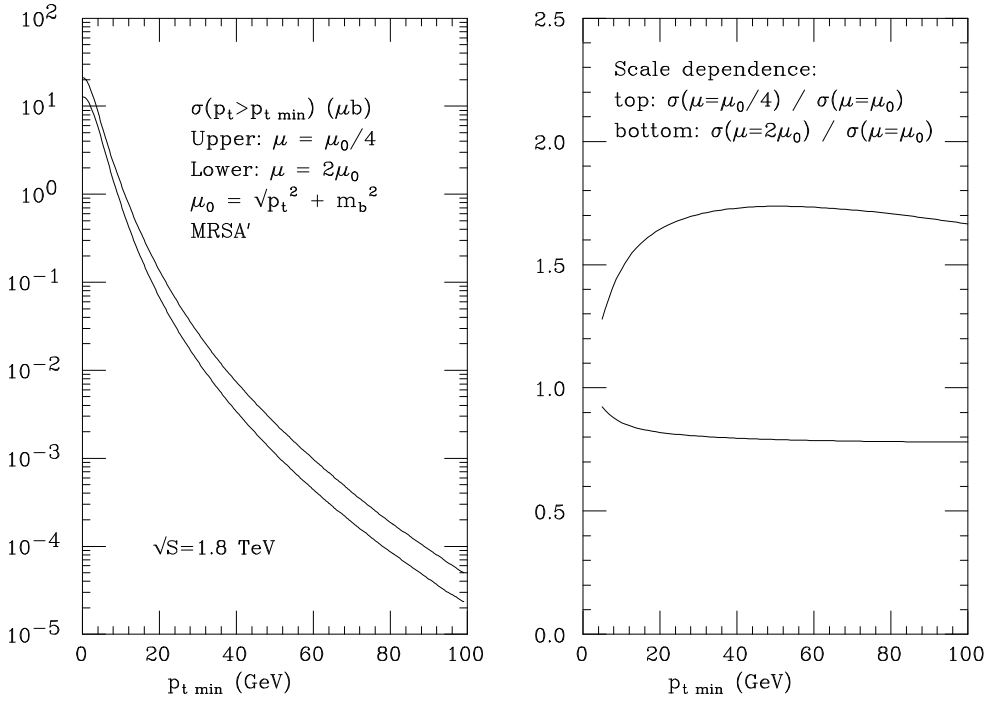

Figure 5: *Scale dependence of the inclusive p_T distributions for bottom quarks, in $p\bar{p}$ collisions at $\sqrt{S} = 1.8$ TeV. $\mu_R = \mu_F = \mu$.*

We can however make some progress in this direction by trying to understand what are the sources of these large NNLO corrections. We can classify them as follows:

- "Accidentals" (e.g. large numerical coefficients, π^2's, etc., which should not affect the scale dependence).
- Large logarithms due to the coexistence of different scales. E.g.:

$$\log \frac{S}{m^2} \quad , \quad \log \frac{p_T^2}{m^2}$$

The origin of these logarithms is known, and will be discussed in the remaining of this lecture. They are universal, namely they are associated to a universal behaviour of the cross-section in some particular kinematic configurations. Because of this, their structure can be predicted at all orders of PT, and in principle they can be resummed. One then hopes that these resummed large logarithms capture all the essential features of the higher-order corrections, and help to improve the behaviour of the perturbative predictions, without the need of a complete NNLO (or even higher-order) calculation.

Before we start analysing the sources of these logarithms in detail, some general comments are in order:

i) No collinear singularities appear when gluons are emitted from the final state heavy quarks, since they are screened by the quark mass. Therefore, contrary to the case of a light parton, $d\sigma/dp_T$ for a heavy quark is a well-defined quantity in NLO. For light partons, one would encounter a collinear singularity and would have to introduce a fragmentation function, usually not calculable from first principles.

ii) At large p_T, nevertheless, large $\log(p_T/m)$ factors appear, signalling the increased probability of collinear gluon emission. At large p_T, the massive quark looks in fact more and more like a massless particle. These logarithms can be resummed using the fragmentation function formalism. Contrary to the case of light quarks, however, the fragmentation function for a heavy quark can be calculated from first principles [15, 16].

iii) New processes appear at NLO which drastically change either the $\hat{s}$ dependence of the cross-sections, or the kinematical distributions.

In the following few subsections I will present some examples of where these large corrections arise, and how they can be accounted for. The discussion will be rather qualitative, and is just meant to give an idea of the main issues and to introduce a nomenclature which is often used in the literature and heard in seminars. I hope these examples will help you demistifying some possibly esoteric language. For more detailed treatments, look at the literature quoted.

2.3.1 t-channel gluon exchange diagrams

Diagrams with a gluon exchanged in the t-channel alter the high-energy behaviour of the total cross-section [7]. Consider for example the following diagram:

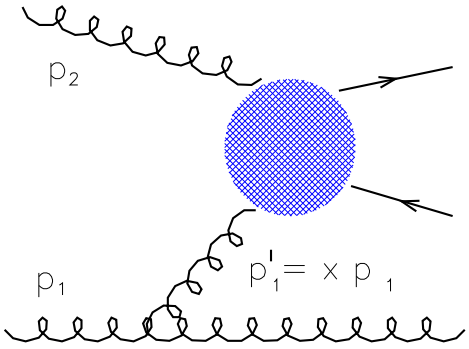

Let us call $\hat{s}$ the incoming total energy squared, and s' the energy squared of the hard subprocess involving gluon 2 and $1'$. Let us concentrate on the phase-space region where $s' \ll \hat{s}$. Since the probability to find the gluon $1'$ with momentum fraction x inside gluon 1 is proportional to α_s/x, the approximate contribution from this process to the heavy-quark cross-section is

$$\sigma_{12\to Q\overline{Q}X} \sim \int_{4m^2/\hat{s}}^1 dx \frac{\alpha_s}{x}\, \sigma(1'2 \to Q\overline{Q}) \tag{23}$$

Using

$$\begin{aligned} \sigma_{1'2\to Q\overline{Q}} &\sim \frac{\alpha_s^2}{s'} = \frac{\alpha_s^2}{x\hat{s}} \\ &\Rightarrow \sigma_{12\to Q\overline{Q}X} \sim \int_{4m^2/\hat{s}}^1 \alpha_s \,\frac{dx}{x^2}\,\frac{\alpha_s^2}{\hat{s}} = \frac{\alpha_s^3}{\hat{s}}\left(\frac{\hat{s}}{4m^2}-1\right) \to \left(\frac{\alpha_s}{4m^2}\right)\alpha_s^2 \end{aligned}$$

Therefore,

$$\frac{\hat{\sigma}_{NLO}(gg\to Q\overline{Q}g)}{\hat{\sigma}_{LO}(gg\to Q\overline{Q})} \overset{\hat{s}\to\infty}{\to} \alpha_s \frac{\hat{s}}{m^2} \tag{24}$$

At very high partonic energies, the NLO process will dominate over the LO one! Of course production at large energy is suppressed in the total hadronic cross-section by the convolution with the steeply falling parton densities. To quantify the impact of these effects, we can take for example a gluon density inside the proton with the form:

$$f(x) \sim \frac{\mathcal{A}}{x^{1+\delta}}$$

with $\delta < 1$ It is then easy to show (Exercise!) that

$$\frac{\sigma_{\rm NLO}(p\bar{p} \to Q\overline{Q})}{\sigma_{\rm LO}(p\bar{p} \to Q\overline{Q})} \sim \begin{cases} \alpha_s \log \frac{S}{4m^2} & \text{if } \delta \log \frac{S}{4m^2} \ll 1 \\ \\ \alpha_s \frac{1+\delta}{\delta} & \text{if } \delta \log \frac{S}{4m^2} \gg 1 \end{cases}$$

Therefore, for small δ the NLO correction becomes larger than the LO term as soon as $\alpha_s \log S/4m^2 \gtrsim 1$. At the Tevatron (and for $m = m_b \sim 4.5$ GeV), this number is indeed of order 1!

These large logarithms are known as "$\log \frac{1}{x}$" terms, where $x \sim \sqrt{4m^2/S}$ is the average value of the hadron energy fraction needed to produce the pair. These $\log 1/x$ terms appear at all orders of PT, but fortunately techniques are known to resum them [17, 18]. Notice, however, that they would not be present if the gluon density were steeper than $1/x$. For example, $\delta = 0.5$ would give only a moderate NLO contribution. The apparent paradox of this different behaviour for different values of δ is resolved by the observation that these large $\log 1/x$ terms can be resummed in a universal fashion and absorbed in an improved evolution equation for the gluon density (the BFKL evolution equation). As a result of this evolution, a gluon density with $\delta = 0$ immediately develops a $\delta > 0$. One can therefore work with a BFKL resummed gluon density, and forget about large $\log(1/x)$ corrections to the heavy-quark production cross-section.

More accurate estimates of the effect of $\log(1/x)$ resummation for b productionat the Tevatron can be found in [18], where it was concluded that corrections of up to 30% in addition to the NLO calculation can be expected.

2.3.2 Gluon-splitting contributions

The so-called gluon-splitting contributions come from diagrams of the following type:

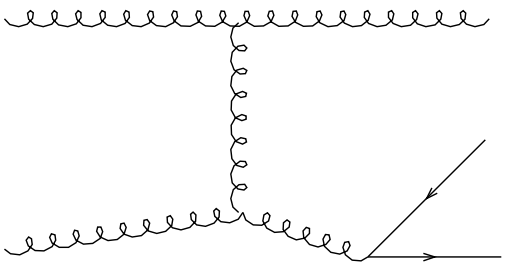

In this case we should focus on the region of phase-space where the t-channel gluon is very hard and far off-shell, while the *splitting* gluon has a virtuality much smaller than its transverse momentum. These diagrams then give rise to potentially large logarithms. We can use a fragmentation-function language to estimate the contribution of these processes to heavy-quark production. One factorizes the process into a $gg \to gg$ (or $qg \to qg$) scattering, with one final-state gluon off-shell, followed by

the evolution of the off-shell gluon into a $Q\overline{Q}$ pair. Higher-order corrections, such as the emission of multiple gluons from the final state gluon, can be included by convoluting the light-parton cross-section with the $g \to Q$ fragmentation function. This approach is similar to what done in the case of inclusive light-hadron production inside a jet, with the difference that the $g \to Q$ fragmentation function can be calculated from first principles within PT [16]. This will account both for the increase in probability that the gluon will turn into a heavy-quark pair (due to the larger number of gluons present when one considers the multi-gluon emission), and for the slow-down of the heavy-quark momentum due to the loss of energy in the multi-gluon radiation process. The fragmentation function for a heavy quark inside a gluon jet with transverse energy $p_\perp$ obeys the evolution equation:

$$\frac{dD(x,q^2)}{d\log q^2} = \frac{\alpha_s}{2\pi}\int_x^1 \frac{dz}{z} G(z,q^2,{p_T}^2) P_{Qg}(\frac{x}{z}) \tag{25}$$

where $G(z,q^2,{p_T}^2)$ is the density of gluons of virtuality q^2 carrying a momentum fraction z inside a gluon of maximal virtuality ${p_T}^2$, and $P_{Qg}(x)$ is the Altarelli-Parisi kernel given by

$$P_{Qg} = \frac{1}{2}[z^2 + (1-z)^2]$$

The heavy-quark multiplicity (which, for small average multiplicity, coincides with the probability to find a quark in the gluon jet) is given by the first moment of the fragmentation function[6]:

$$N \equiv \int_0^1 dz D(z) \tag{26}$$

which obeys the equation:

$$\frac{dN}{d\log q^2} = \frac{\alpha_s}{2\pi} G_{(1)} P_{Qg}^{(1)}$$

with $G_{(1)}$ and $P_{Qg}^{(1)}$ first moments of $G(x)$ and $P_{Qg}(x)$. $G_{(1)}(q^2,{p_T}^2)$ is the number of gluons with virtuality q^2 in the jet, and

$$P_{Qg}^{(1)} = \int_0^1 dz\ \frac{1}{2}(z^2+(1-z)^2) = \frac{1}{3}\ .$$

At the first order, neglecting the q^2-dependence of the gluon multiplicity and therefore assuming $G_{(1)} \equiv 1$, we get

$$N(Q\bar{Q}) \sim \frac{\alpha_s}{6\pi}\log\left(\frac{p_T^2}{m^2}\right) \tag{27}$$

where p_T^2 and m^2 are the maximum and minimum gluon virtuality. In the case of light quarks, $m = 0$ and this calculation would not be possible. A collinear divergence would develop, associated to the vanishing minimum gluon virtuality, and one would need to introduce a non-perturbative fragmentation function. Once more, this shows the advantage of working with heavy quarks!

The logarithm in eq. (27) signals the growth in probability to find a heavy quark inside a large-p_T gluon. It is yet one more potentially large logarithm that was not present at leading order, and which appears for the first time at NLO. Similar large logarithms will appear at higher orders of perturbation theory (associated to processes where more gluons are radiated in the final state). These logarithms are resummed by solving exactly the evolution equation for the $g \to Q$ fragmentation function, eq. (25).

[6]The n-th moment of a function $f(x)$ is defined by $\int_0^1 dx\ x^{n-1} f(x)$.

2.3.3 Flavour-excitation processes

An analogous class of NLO corrections is given by the so-called *flavour-excitation* diagrams. These can be thought of as initial-state gluon-splitting processes:

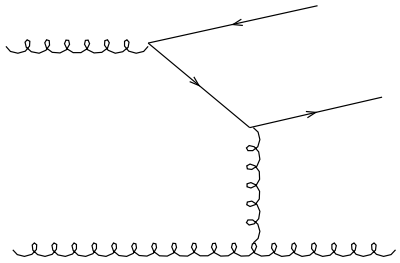

The relevant region of phase-space in this case is the one with the heavy-quark propagator close to the mass shell. These processes are analogous to the singlet contribution to F_2 in DIS. It is known that these effects can be reabsorbed in the AP evolution of the parton densities [19]. In our case, this is equivalent to defining a heavy-quark density inside a proton by:

$$\begin{cases} \frac{dD_Q(x,q^2)}{d\log q^2} &= \frac{\alpha_s}{2\pi}\int_x^1 \frac{dz}{z} G(z,q^2) P_{Qg}\left(\frac{x}{z}\right) \\ D_Q(x,m^2) &= 0. \end{cases} \tag{28}$$

It is easy to get a crude estimate of the "heavy-quark density" by assuming a simple functional form for $G(x)$, for example, $G(x) = A/x$. Then:

$$\begin{aligned} \frac{dD_Q(x)}{d\log q^2} &= \frac{\alpha_s}{2\pi}\int_x^1 \frac{dz}{z}\, G\left(\frac{x}{z}\right)\, P_{Qg}(z) \\ &= \frac{\alpha_s}{2\pi}\int_x^1 \frac{dz}{z}\, \frac{A}{x/z}\, \frac{1}{2}\left[z^2+(1-z)^2\right] \\ &\simeq \frac{\alpha_s}{6\pi} G(x) \end{aligned}$$

Assuming $G(x,q^2)$ slowly varying in the $q^2 \gtrsim m^2$ region:

$$\boxed{D_Q(x,q^2) \simeq \frac{\alpha_s}{6\pi}\log\left(\frac{q^2}{m^2}\right) G(x,q^2)}$$

Since the NLO corrections contain these "structure function-like" piece, it would be incorrect to add to LO processes contributions from $gQ \to gQ$. In fact, this would imply a double-counting of the NLO flavour-excitation diagrams. Of course, the use of the $gQ \to gQ$ process allows one to capture higher-order effects included in the AP evolution equations, which are usually solved to generate the heavy-quark densities found in standard Fortran libraries of parton density functions. The use of the NLO flavour-excitation diagrams reproduces instead more faithfully the exact kinematics and correlations of the flavour-creation process in the region next to the threshold.

The example I will give here describes the comparison between the two approaches when applied to the simpler case of associated production of a γ and heavy quarks. In this case I

compare the results of the two calculations of the photon $p_\perp$ spectrum obtained by using either of the these two processes:

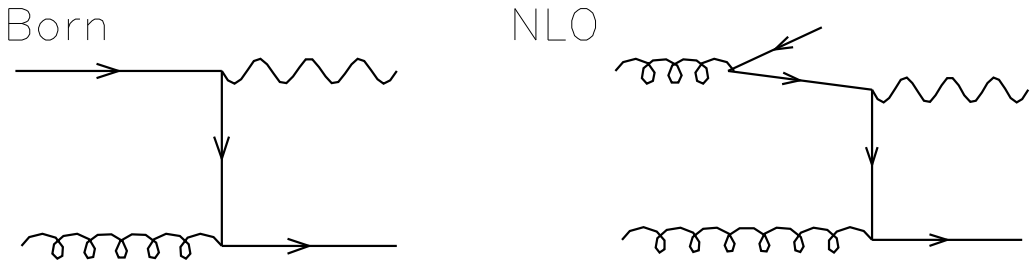

The calculation done using the LO approach, which uses as an input the b structure function taken from a given set of parton distribution functions (CTEQ1M, in this case), is shown in fig. 6 as a solid line. The calculation done by evaluating the $\mathcal{O}({\alpha_s}^2\alpha_{\rm EM})$ matrix element is shown by the dashed line. The ratio of the two distributions is given in fig. 7. Notice that the two calculations agree remarkably well down to low values of p_T, indicating that even the structure function approach can be used to reproduce rather accurately the onset of the mass threshold (this is because we are looking at a rather inclusive quantity. Were we looking at more exclusive quantities, or at correlations between the b and the $\bar{b}$ in the final state, the LO approach would not even be usable: in this approach the antiquark is always integrated over and we cannot keep track of where it went!) At large p_T some differences between the two calculations emerge, due to the absence of higher-order terms in the NLO calculation. These higher-order terms are included in the structure-function approach, since the b structure function itself has been evolved to large p_T using the exact Altarelli-Parisi evolution equation. The ideal calculation, therefore, would merge the two approaches by smoothly interpolating betwen the two regimes. This was done in refs. [20, 21], and the results will be discussed in the next lecture.

2.4 Heavy-quark fragmentation

At the end of the perturbative evolution, one still expects hadronization effects to alter the spectrum of the heavy quark while it transforms into a hadron. These effects are usually described in terms of a non-perturbative fragmentation function. The fundations of this approach lie in a *factorization theorem*:

$$\frac{d\sigma}{dP_T} \;=\; \int_{\frac{P_T}{E_{beam}}}^1 \frac{dz}{z}\, F(z)\, \frac{d\sigma}{dp_t}(p_t = P_T/z)$$

where P_T is the hadron momentum, and $d\sigma/dp_t$ includes the *perturbative* part of the heavy-quark fragmentation function, namely the resummation of the $\log(p_T/m)$ terms [16]. The factorization theorem ensures that, up to corrections of order Λ/P_T, with Λ a scale typical of the hadronization phenomena, the function $F(z)$ for a given heavy flavour is universal. Although non-perturbative in nature, some general features of fragmentation functions can be extracted from first principles. For example, one can establish a relation between the effects of hadronization on heavy quarks of different masses:

$$1 - \bar{x}_B = \left(\frac{m_c}{m_b}\right)(1 - \bar{x}_D) \tag{29}$$

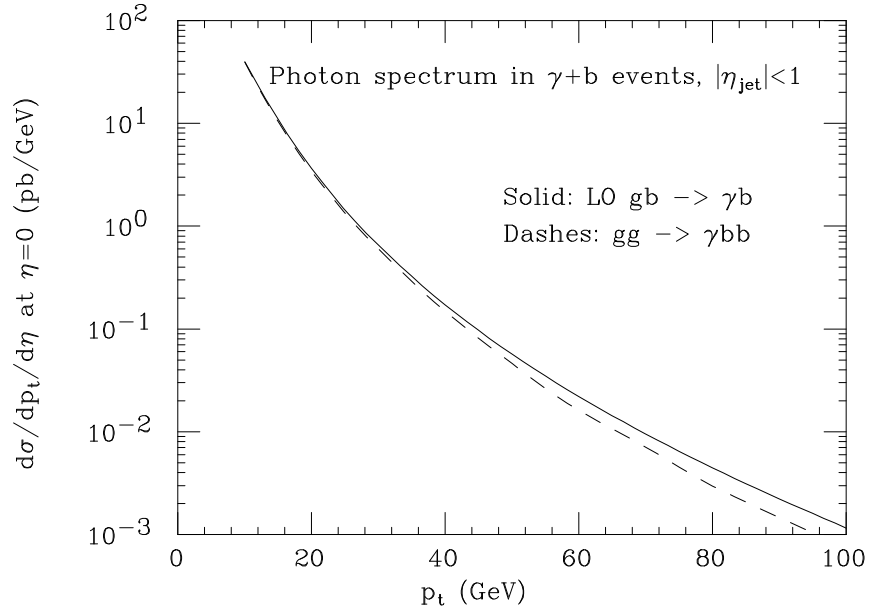

Figure 6: *The p_T distributions for central photons produced in association with a b quark, in $p\bar{p}$ collisions at $\sqrt{S} = 1.8$ TeV. The results of the two different calculations discussed in the text are displayed.*

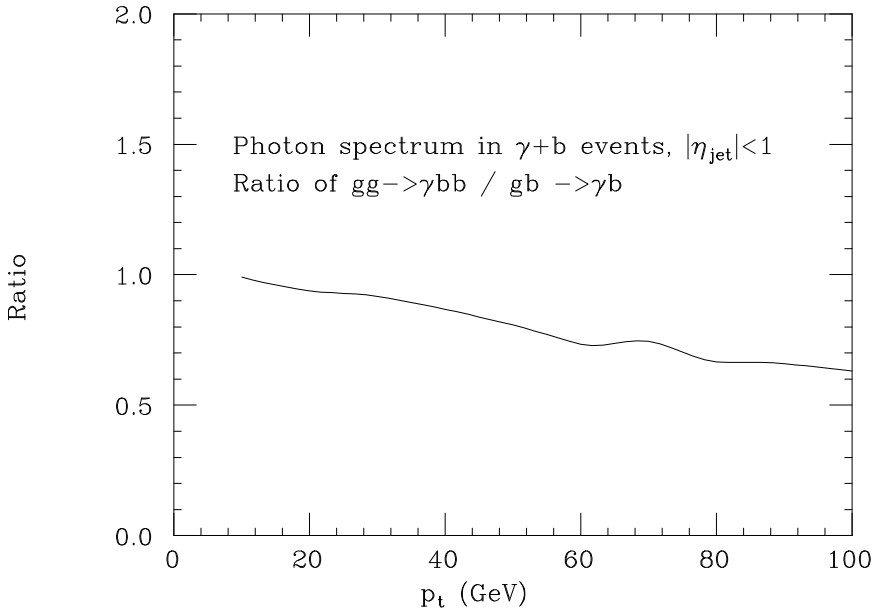

Figure 7: *The ratio between the two curves shown in the previous figure.*

where $\bar{x}$ is any parameter such as $\langle x \rangle$ (the average value of x) or $x_{\rm max}$ (the value of x at which the fragmentation function peaks). This follows easily from phase-space considerations. One can idealize the fragmentation process with a transition of a slightly off-shell heavy quark (possibly in the field of nearby soft gluons) decaying to a heavy hadron H plus a light system Π (e.g. pions):

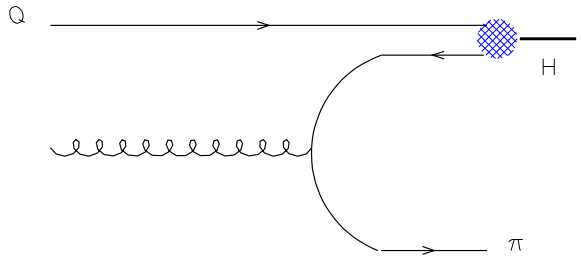

In this case:

$$P_H \ : \ P_\Pi \ \equiv \ z_H \ : \ z_\Pi \ = \ M_H \ : \ M_\Pi \tag{30}$$

and, as a result,

$$1 - z \sim 1 - \frac{M_H}{M_H + M_\Pi} \sim \frac{M_\Pi}{M_H} \tag{31}$$

A typical example of parametrizations for non-perturbative fragmentation functions is the *Peterson, Schlatter, Schmitt* and *Zerwas* form [22]:

$$\frac{dN}{dz} \propto \frac{1}{x\left[1 - 1/x - \epsilon/(1-x)\right]^2} \tag{32}$$

Here ϵ is the only parameter describing the non-perturbative part, and scales as follows:

$$\epsilon \sim \frac{m_0^2}{m_Q^2} \qquad \langle 1 - z \rangle \sim \sqrt{\epsilon} \tag{33}$$

Another interesting form was proposed by *Nason* and *Colangelo* [23]:

$$\frac{dN}{dz} \propto (1-z)^\alpha \ z^\beta \tag{34}$$

In this case the relation between the values of α and β for different values of the heavy-quark mass (say charm and bottom hadrons) can be extracted by imposing the two relations:

$$1 - \langle x_B \rangle \ = \ \frac{m_c}{m_b}(1 - \langle x_D \rangle) \tag{35}$$

$$1 - \hat{x}_B \ = \ \frac{m_c}{m_b}(1 - \hat{x}_D) \ , \tag{36}$$

which can be easily solved analitically (Exercise!) in terms of α and β. The values of the parameters characterizing the non-perturbative fragmentation functions can be extracted by fitting some set of data. The factorization theorem will then allow us to use the same parameters to predict cross-sections for other data. The best place to extract information on heavy-quark fragmentation is e^+e^- collisions, since there at least the energy of the primary heavy quark before the

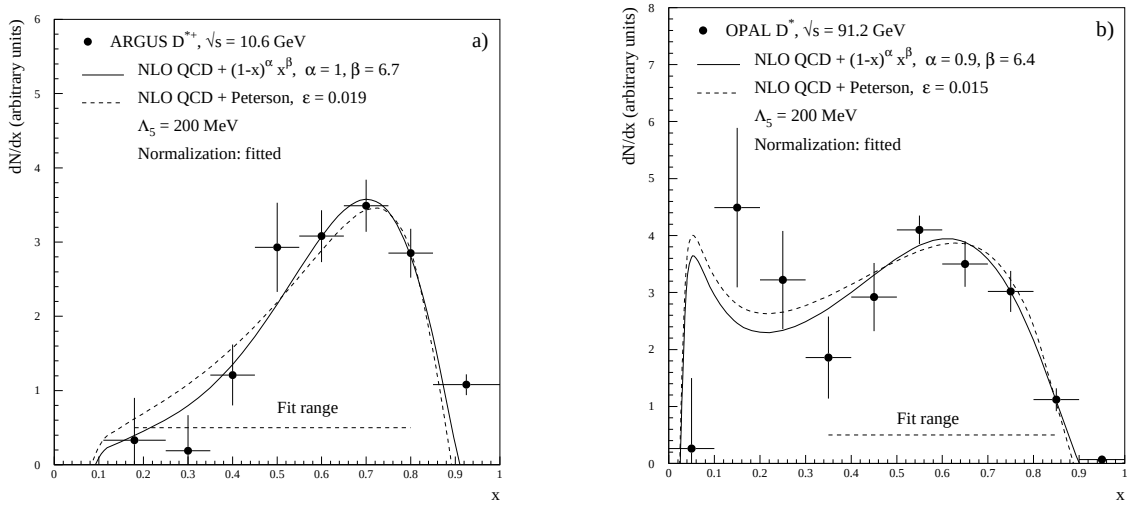

Figure 8: *Fits to the charm fragmentation function measured at ARGUS (left) and OPAL (right).*

perturbative and non-perturbative fragmentation processes occur is well determined, being equal to the beam energy. Recent fits to charm production data from the old ARGUS experiment [24] at DESY ($\sqrt{s} = 10.6$ GeV) and the more recent OPAL experiment [25] at LEP ($\sqrt{s} = 91.2$ GeV) have been performed in ref. [26]. The results are shown in fig. 8. The parameters extracted from the fits to the data of the two experiments, using different values of Λ_{QCD}, are contained in the following tables (for ARGUS and OPAL, respectively):

Λ_5=200 MeV	300 MeV
ϵ_c=0.019	0.011
$\alpha = 1$	-
$\beta = 6.7$	-

Λ_5=200 MeV	300 MeV
ϵ_c=0.015	0.008
$\alpha = 0.9$	-
$\beta = 6.4$	-

Few comments should be made:

- There is a very good agreement between the value of the parameters extracted from the two experiments. This confirms the validity of the factorization theorem.
- The value of the parameters depends strongly on the input value of Λ_{QCD}. This is reasonable, since the perturbative part of the heavy-quark evolution will depend on the strength of the perturbative coupling constant α_s. A larger value of α_s implies a larger amount of energy radiated off in the form of gluons. This leaves less energy to the quark before it hadronizes, and calls for a harder non-perturbative fragmentation to reproduce the data than if a small value of α_s were used to start with. This correlation is faithfully reproduced by the fits shown above. Notice also that the value of the Peterson parameter ϵ_c which is usually obtained by using the LO result for the perturbative part of the fragmentation function ($\epsilon_c = 0.06$, [26, 27]), is much larger than what extracted from these NLO fits ($\epsilon_c = 0.01 - 0.02$).

The relations given in eqs. (35-36) allow us to predict the value of the parameters governing the non-perturbative fragmentation of b quarks. When this is done, one can predict the b-hadron

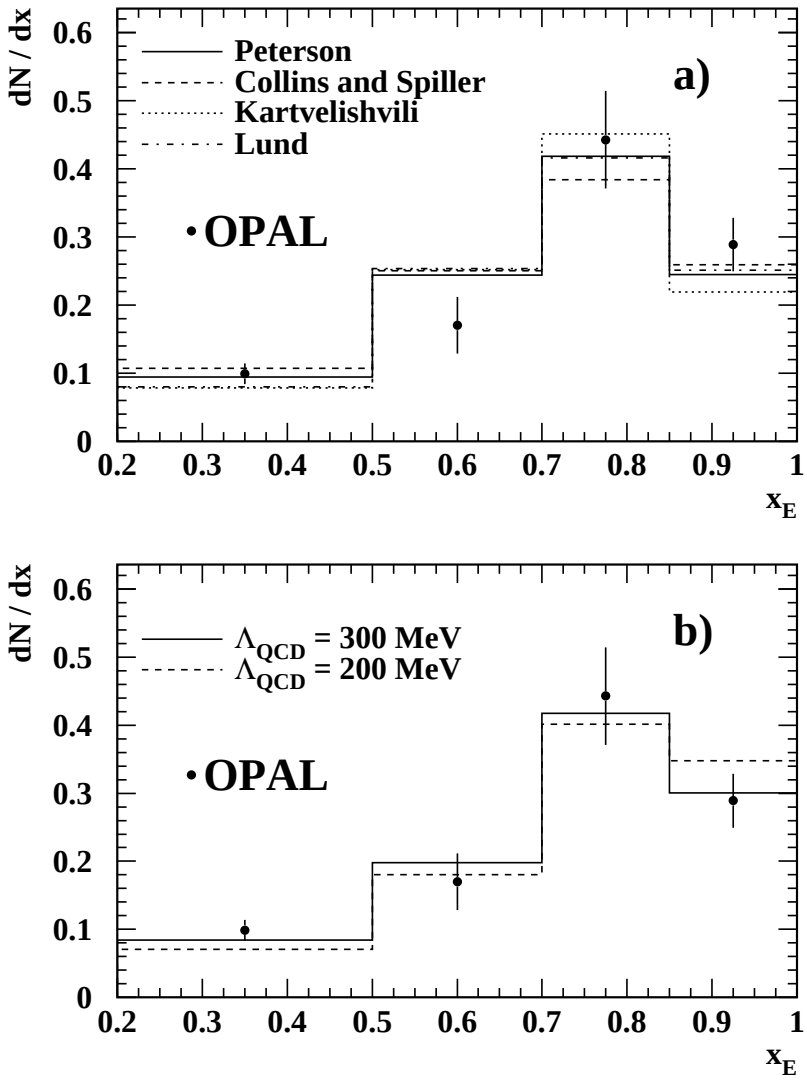

Figure 9: *Comparison of OPAL b-fragmentation function data with* fits *to different fragmentation function forms (upper figure), and with* predictions *based on the convolution of the b-quark NLO fragmentation function and the Colangelo-Nason non-perturbative fragmentation function, with parameters extrapolated from fits to the charm fragmentation function (lower figure).*

fragmentation function at LEP. The comparison of data [28] and theory (using the Colangelo and Nason fragmentation model, and the α and β values extracted from the charm fits) is shown in the bottom plot of fig. 9. Excellent agreement is seen, again a good test that we are on the right track!

3 Phenomenology of heavy-quark production

The ultimate test of our ability to describe the heavy-quark production processes rests on the comparison with actual data. In the remaining part of these lectures I will present a survey of current experimental results, and how they compare to theory. Unless otherwise indicated, *theory*

will refer to NLO calculations. A more complete review can be found in ref. [29].

3.1 Fixed target production

Heavy-flavour production has been studied extensively in fixed-target experiments, with both hadron and photon beams. The typical centre-of-mass energy is in the range 10-40 GeV, where the bottom cross-section is rather small. Therefore most of the available data are on charmed-hadron production. Total cross-sections, single-inclusive distributions, correlations between the quark and the antiquark have been measured in both hadro- and photoproduction. The theoretical apparatus of perturbative QCD is in this case at its very limit of applicability, because the charm mass is very close to typical hadronic scales. Thus, effects of non-perturbative origin will very likely play an important role. Conversely, it is hoped that these effects may be better understood by studying charm production. Although modern fixed-target experiments have considerably improved the situation, many open problems remain in this field. All experimental results are in qualitative agreement with perturbative QCD calculations, thus supporting the "hard" nature of charm-production phenomena. However, several quantitative deviations from pure QCD are observed. It is interesting to see whether simple models of non-perturbative phenomena, such as fragmentation effects and intrinsic transverse momenta, may be sufficient to explain these deviations. I will discuss these problems at length. I will not discuss, instead, the subject of x_F-asymmetries. A discussion of this issue can be found in ref. [29], and recent relevant data (and references to previous literature), in ref. [30].

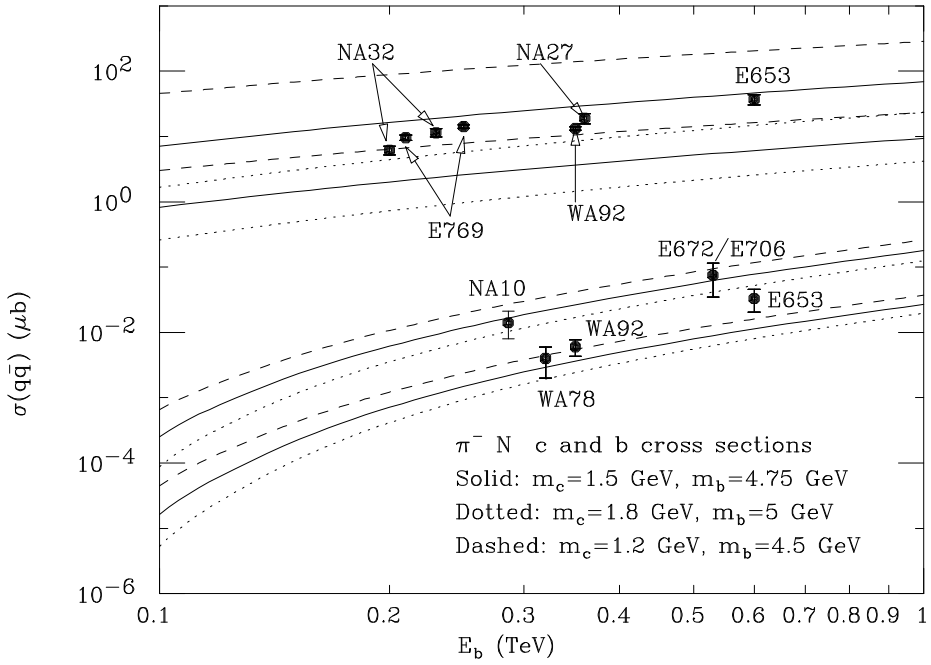

Figure 10: *Pair cross-sections for b and c production in $\pi^- N$ collisions versus experimental results.*

3.1.1 Total cross-sections

In fig. 10 I plot the $c\bar{c}$ and $b\bar{b}$ cross-sections, computed in QCD at NLO, as functions of the beam energy, for $\pi^- N$ collisions. The same quantities are shown in fig. 11 for a proton beam. The cross-sections are calculated using the parton distribution sets of ref. [31] for the nucleon, and the central set SMRS2 [32] for the pion. The default values of the charm and bottom masses are 1.5 and 4.75 GeV respectively, and the default choices for the factorization scale $\mu_{\rm F}$ and the renormalization scale μ_R are

$$\mu_{\rm F} = 2m_c, \quad \mu_R = m_c \quad \text{and} \quad \mu_{\rm F} = \mu_R = m_b \tag{37}$$

for charm and for bottom.

The bands in the figures are obtained as follows. We varied μ_R between half and twice the central value. The factorization scale $\mu_{\rm F}$ was also varied between $m_b/2$ and $2m_b$ in the case of bottom, while it was kept fixed at $2m_c$ in the case of charm. This is because the adopted parametrizations of parton densities are given for Q^2 larger than 5 GeV^2. The bands shown in the figures are therefore only an underestimate of the uncertainties involved in the computation of charm production cross-sections. Considering independent variations for the factorization and renormalization scales does not lead to a wider range in the bottom cross-section for the energies shown in the figures. We also show the effect of varying m_c between 1.2 GeV and 1.8 GeV, and m_b between 4.5 and 5 GeV.

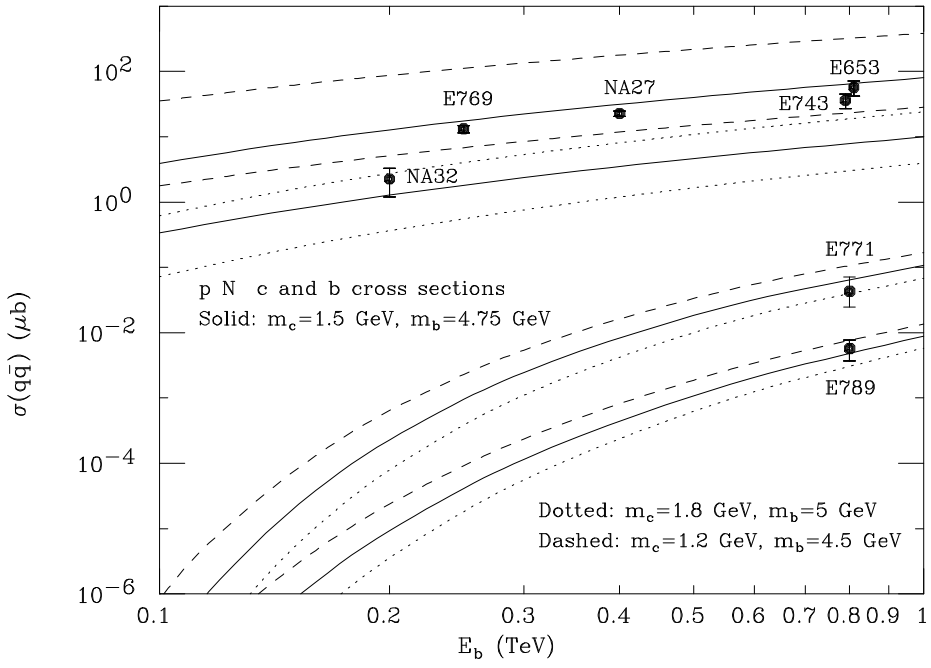

Figure 11: *Pair cross-sections for b and c production in pN collisions versus experimental results.*

The proton parton densities of ref. [31] are available for a wide range of $\Lambda_{\rm QCD}$ values, corresponding to $\alpha_s(m_{\rm Z})$ values between 0.105 and 0.130. The bands shown in figs. 10 and 11 for

bottom production are obtained by letting $\Lambda_{\rm QCD}$ vary in this range. In the case of charm, values of $\Lambda_{\rm QCD}$ corresponding to $\alpha_s(m_Z)$ above 0.115 induce values of $\alpha_s(m_c)$ too large to be used in a perturbative expansion. For this reason, the upper bounds on charm production cross-sections are obtained with $\alpha_s(m_Z) = 0.115$. We point out that, by varying $\Lambda_{\rm QCD}$, one is forced to neglect the correlation between $\Lambda_{\rm QCD}$ and the pion parton densities, which were fitted in ref. [32] with $\Lambda_5^{\overline{\rm MS}} = 122$ MeV.

As can be seen, experimental results on total charm cross-sections [33, 34, 35, 36, 37, 38] are in reasonable agreement with theoretical expectations, if the large theoretical uncertainties are taken into proper account. We can see that the hadroproduction data are compatible with a value of 1.5 GeV for the charm-quark mass. In the case of bottom production [39], the spread of the experimental data is almost as large as that of the theoretical predictions. The two results in proton-production [40, 41] differ at the level of 2.5σ. This is unfortunate, since the beam energy ($E_p = 800$ GeV) is almost the same of the forthcoming HERAB experiments. A more consistent experimental estimate of the production cross-section would have provided more reliable estimates of the b rate at HERAB.

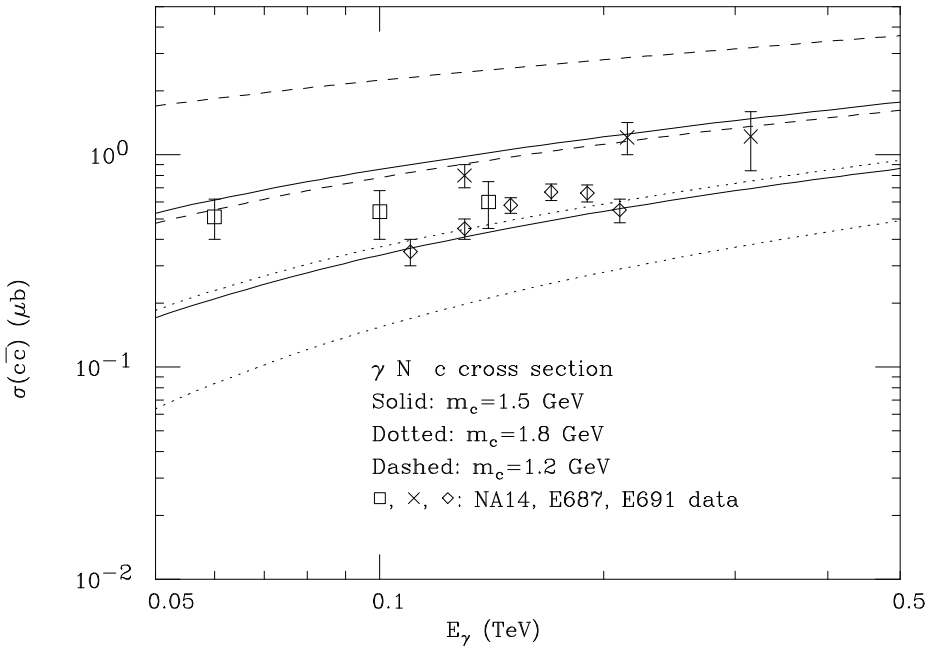

Figure 12: *Pair cross-sections for c production in γN collisions versus experimental results.*

Total cross-sections for charm production have also been measured in photoproduction experiments. In fig. 12 the relevant experimental results of refs. [42, 43, 44, 45] are shown in comparison with NLO QCD predictions. As can be seen, the theoretical uncertainties are smaller in this case than in the hadroproduction case. Again, a charm mass of 1.5 GeV is compatible with photoproduction data. It should be stressed however that some of the experimental results are incompatible with one another. Until these discrepancies are resolved, it will not be possible to use the data to constrain physical parameters. For example, while the E687 data are inconsistent with a charm

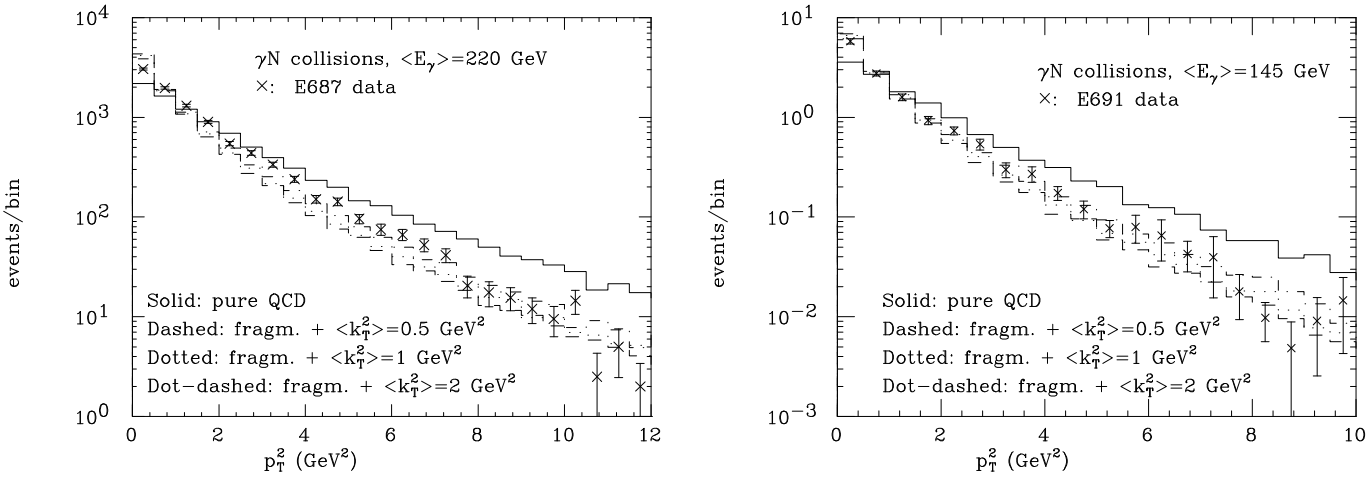

Figure 13: *Experimental p_T^2 distribution compared to the NLO QCD predictions (m_c = 1.5 GeV), with and without the inclusion of non-perturbative effects, in γN collisions.*

mass of 1.8 GeV, this mass value cannot be excluded because of the E691 data.

3.1.2 Single-inclusive distributions

While total cross-section measurements are certainly important, it is equally important to explore in more detail the production properties of heavy quarks. In addition to the theoretical interest, this is relevant to guarantee that some of the experimental systematics (such as the detector acceptances and efficiencies) are under control. When experiments measure total cross-sections, they often do so by probing a fraction of the full available phase-space, and correcting later for the remaining part of phase-space. This is done by using a theoretical modeling of the differential distributions. Checking that these agree with the data is therefore a fundamental test.

Many experiments have measured single-inclusive x_F and p_T distributions for charmed hadrons in πN collisions [33, 46, 47, 48, 49] and in pN collisions [36, 37, 38, 48]. Distributions are expected to be more affected by non-perturbative phenomena than total cross-sections. For example, an intrinsic transverse momentum of the incoming partons, and the hadronization of the produced charm quarks, may play an important rôle in this case. We will therefore try to assess the impact of such phenomena by means of simple models.

I start by presenting in fig. 13 the p_T^2 distributions measured in photon–nucleon collision by the E687 [45] and by the E691 [43, 44] collaborations. I also show the NLO QCD prediction for bare quarks (the solid histogram), which as you can see is significantly harder than the data[7]. This is reasonable, since the non-perturbative fragmentation of the charm quark into a charmed hadron will reduce the hadron momentum relative to the quark one. As discussed in the previous lecture, we can describe this slow-down by including a non-perturbative fragmentation function. The dashed and dotted histograms in the figures include the convolution with a Peterson fragmentation function (as well as with an intrinsic transverse momentum, k_T, as will be discussed in a moment). We chose here the standard value of $\epsilon_c = 0.06$, which was used in [29]. The agreement with the data is good.

[7] In this subsection the relative normalization of experimental distributions and theoretical curves has been fixed in order to give the same total rate.

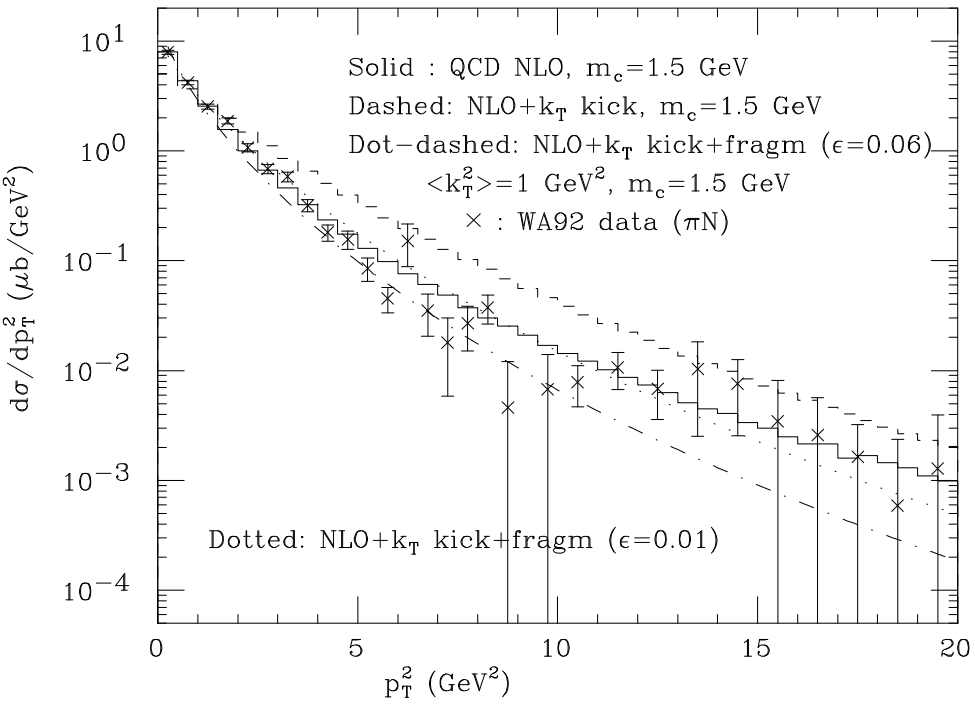

Figure 14: *The single-inclusive p_T^2 distribution measured by WA92, compared to the NLO QCD predictions, with and without the inclusion of non-perturbative effects.*

Let us consider now the case of hadroproduction, and focus on a recent measurement of the single-inclusive differential cross-sections performed at CERN by the WA92 collaboration [35], which uses a π^- beam of 350 GeV colliding with isosinglet nuclei. Consistent results are obtained by using the E769 collaboration [50] data, using pion, proton and kaon beams of 250 GeV on isosinglet targets, and more recent E706 data [51] using 515 GeV pion beams.

In fig. 14 I show the comparison between the single-inclusive p_T^2 distributions measured by WA92 and the theoretical predictions. The solid curve represents the pure NLO QCD prediction for charm quarks, and as you see it almost exactly goes through the experimental points. But this is not necessarily a good sign, since we just learned in the study of photoproduction that we need to include an important effect due to the non-perturbative fragmentation. The factorization theorem discussed in the previous lecture tells us that these effects should be present regardless of the nature of the beam, and once we find out that they must be there in photoproduction, we should include them in hadroproduction as well. We would therefore expect that the final theoretical prediction, including the fragmentation effects, will not agree with the data. Fortunately there is one more effect of non-perturbative origin which comes to our rescue. That is the famous *intrinsic* k_T. Partons inside the proton cannot have rigorously zero transverse momentum, because of the Fermi motion. It has been known for a long time, mainly from the measurement of Drell-Yan events, that quarks in the proton have an average intrinsic k_T of the order of 700 MeV. The dot-dashed line in fig. 14 is obtained by convoluting the quark-level results with the same Peterson fragmentation function used in the case of photoproduction, and with a gaussianly distributed intrinsic k_T, with $\langle k_T^2 \rangle = 1$ GeV^2. This is a reasonable choice for $\langle k_T^2 \rangle$, since gluons can be

expected to have a braoder k_T distribution than quarks.

As you can see the effects of fragmentation and of the intrinsic k_T almost completely cancel each other, and leave a p_T^2 distribution which is in fair agreement with the data. If we use the value of the Peterson parameter ϵ_c extracted from the recent fits described in the first lecture, $\epsilon_c = 0.01$, we obtain an even better agreement (see the dotted line in fig. 14). Notice that in the photoproduction case the p_T^2 distribution is less sensitive to the choice of $\langle k_T^2 \rangle$. This is because in photoproduction only one of the two initial-state particles (i.e. the gluon) can have an intrinsic k_T, while in the hadroproduction case both of them do. This reduced sensitivity is shown in fig. 13: the curves with $\langle k_T^2 \rangle = 2$ GeV^2 and $\langle k_T^2 \rangle = 1$ GeV^2 are not significantly different from one another.

Having determined the values (or at least a range of values) for the non-perturbative parameters which we expect should describe the production of charm quarks at large p_T, we must now proceed and see whether the remaining possible distributions that can be predicted do agree with the data or not. If they did not, this would be an indication that there are extra phenomena at play which we have not accounted for.

3.1.3 Correlations in fixed-target production

A distribution which is very sensitive to the presence on a non-perturbative k_T-kick is the azimuthal correlation between the quark and the antiquark. This is clear because already at LO, where the quarks are produced back-to-back in the transverse plane and the $\Delta\phi$ distribution is a sharp peak at 180°, any transverse kick to the system will drastically change the topology of the final state. Many experimental results on correlations between charmed particles in hadro- and photoproduction have been obtained by different experiments (see for example refs. [52, 53, 38, 54, 55, 49, 56, 57]); these reported distributions of the azimuthal distance between the charmed hadrons, the rapidity difference, the invariant mass and the transverse momentum of the pair. A detailed comparison of these results with QCD predictions is performed in ref. [29]. More recently, new measurements of the azimuthal distance and pair transverse momentum for charmed mesons have been presented by the WA92 collaboration [58]. In what follows we will focus on the distribution of $\Delta\phi$, defined as the angle between the projections of the momenta of the pair onto the transverse plane, and of the transverse momentum of the pair $p_T(Q\overline{Q})$. We will discuss whether NLO QCD predictions can describe the available experimental data.

In leading-order QCD the heavy-quark pair is produced in the back-to-back configuration, corresponding to $\Delta\phi = \pi$ and $p_T(Q\overline{Q}) = 0$. NLO corrections, as well as non-perturbative effects, can cause a broadening of these distributions, as illustrated in ref. [59] and [29].

We have chosen, as an illustration for hadroproduction, the cases of the WA75 and the WA92 results, which have both been obtained in $\pi^- N$ collisions at the same energy, $E_b = 350$ GeV. Let us first consider the $\Delta\phi$ distribution. In fig. 15 we show (solid curves) the NLO result superimposed on the data of the two experiments. The charm mass was set to its default value, $m_c = 1.5$ GeV. In both cases, we see that the experimental data favour a much broader distribution than the pure NLO QCD result for charm quarks.

One should, however, take into account also non-perturbative effects, as in the case of single-inclusive distributions. The dashed and dotted curves in fig. 15 correspond to the NLO prediction, supplemented with the effect of an intrinsic transverse momentum with $\langle k_T^2 \rangle = 0.5$ GeV^2 and $\langle k_T^2 \rangle = 1$ GeV^2, respectively. We see that with $\langle k_T^2 \rangle = 0.5$ GeV^2 it is impossible to describe the WA75 and WA92 data. This conclusion differs from the one of ref. [60] for the WA92 result. This

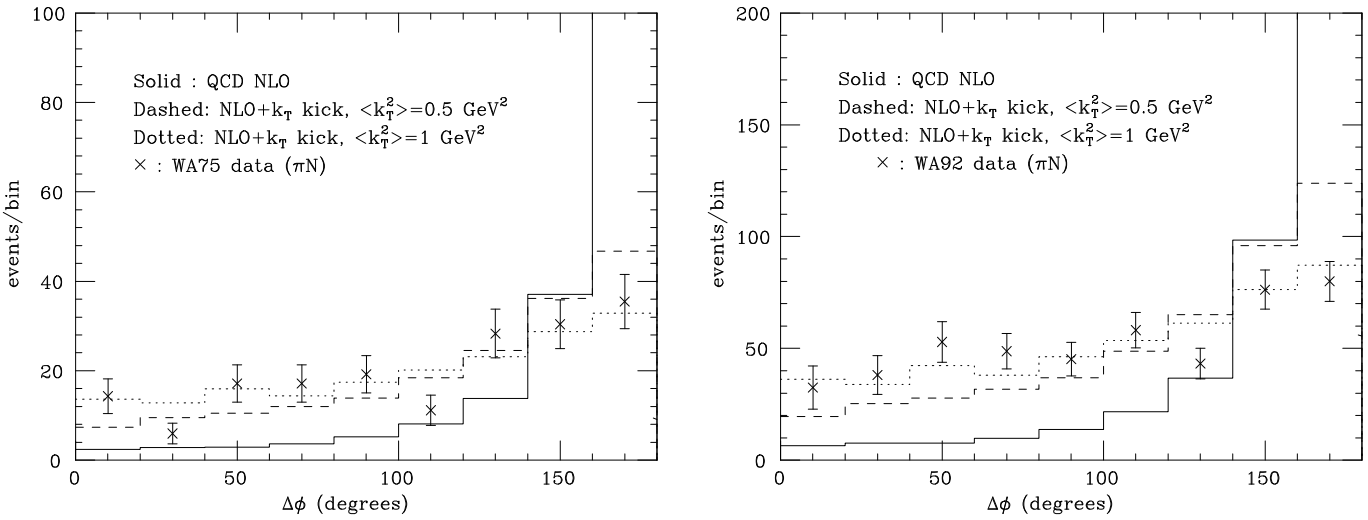

Figure 15: *Azimuthal correlation for charm production in πN collisions: NLO calculation versus the WA75 and WA92 data.*

is because in ref. [58] the WA92 collaboration has improved the study of correlations with respect to ref. [61] by considering a wider set of correlation variables and by improving the statistics by a factor of 5. WA92 and WA75 data now appear to be consistent with each other. As is apparent from fig. 15, the acceptable value of $\langle k_T^2 \rangle = 1$ GeV^2 is required to describe the data. This is encouragingly consistent with the results we obtained form the study of the inclusive-p_T distributions!

The WA75 collaboration, and recently the WA92 collaboration, published in refs. [49, 58] the distribution of the transverse momentum of the heavy-quark pair. This is yet another independent variable, which is sensitive to both intrinsic k_T and fragmentation effects. The theoretical prediction supplemented with a k_T-kick with $\langle k_T^2 \rangle = 1$ GeV^2 cannot reproduce the WA75 data. This is a typical example of why, until recently, no coherent overall picture of the mechanisms at play in charm production was available. The most recent results from WA92, however, confirm the indications of the QCD calculations supplemented with k_T-kick and fragmentation, as displayed in fig. 16. Similar conclusions can be drawn from the study of photoproduction correlation data (the $\Delta\phi$ distributions are shown in fig. 17, the distribution in the transverse momentum of the heavy-quark pair in fig. 18). In all cases $\langle k_T^2 \rangle$ values of the order of 1 GeV^2 are necessary (and sufficient!) to describe the data.

Conclusions:

- For the first time since the beginning of charm production studies we have reached a compelling and coherent picture of the production dynamics in fixed-target experiments. Large data-sets and state-of-the-art detector technology have been fundamental to make outstanding progress in the quality of the data!

- The production dynamics are well described by NLO QCD, supplemented with simple phenomenological descriptions of the NP effects:

  – fragmentation at large p_T

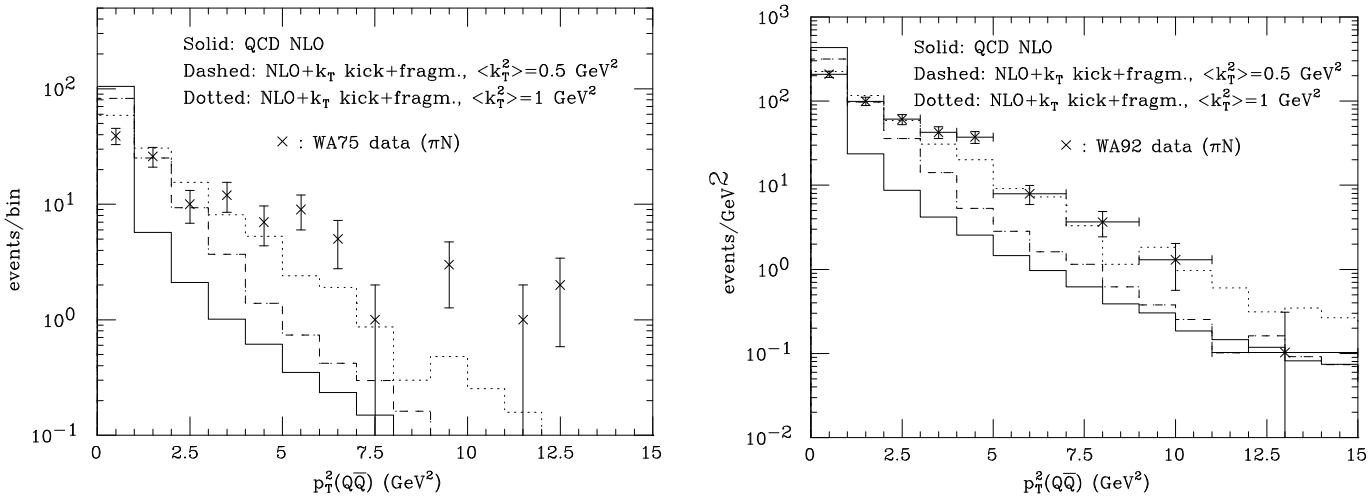

Figure 16: *NLO QCD result for the $p_T^2(Q\overline{Q})$ supplemented with an intrinsic transverse momentum for the incoming partons, compared with the WA75 (left) and WA92 (right) data.*

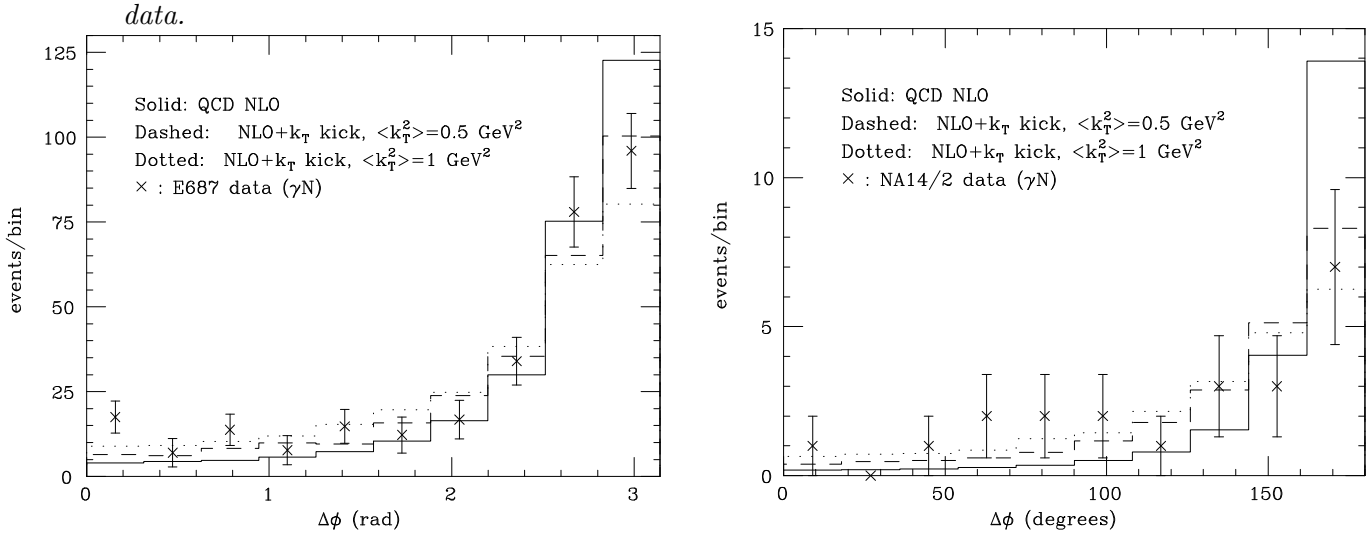

Figure 17: *Azimuthal correlation of $D\bar{D}$ pair versus the perturbative result in photoproduction for the E687 (left) and NA14/2 (right) experiments.*

  - intrinsic $\langle k_T^2 \rangle = 1$ GeV^2

- The parametrization of these effects satisfies the expected universality properties: no dependence on
  - beam type and energy
  - observable
- Additional fine tuning will be possible when more data will be available. We can then expect to sort out the interplay between QCD and NP parameters in a more accurate fashion. E.g.:
  - larger $\alpha_s \rightarrow$ smaller $\langle k_T^2 \rangle$ (from $\Delta\phi$ spectrum)

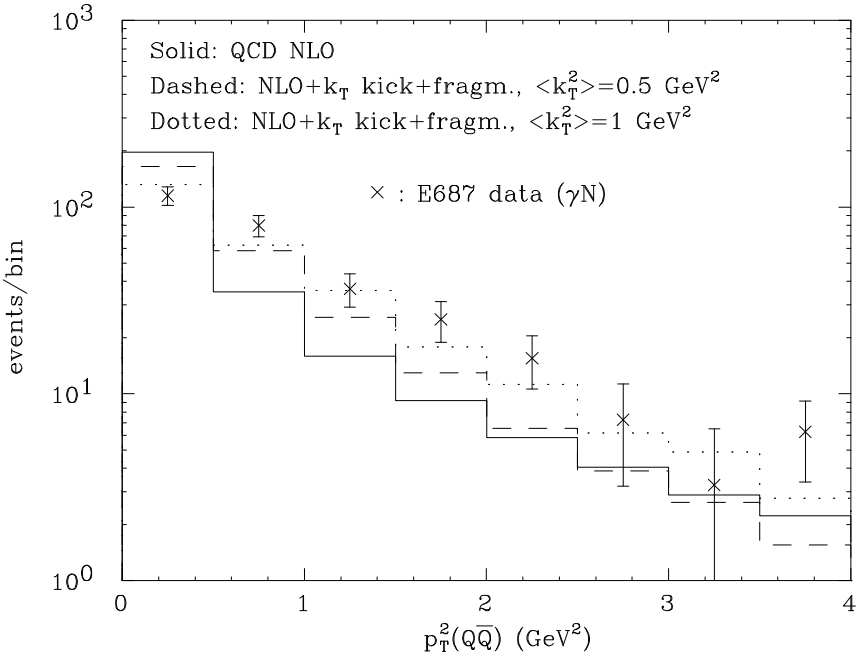

Figure 18: *Transverse momentum distribution of the $D\bar{D}$ pair versus the perturbative result for the E687 experiment.*

– smaller $\langle k_T^2 \rangle \rightarrow$ softer fragmentation (from p_T spectra)

3.2 Heavy-quark production at hadron colliders

Hadron collisions are by far the largest source of heavy quarks available today. While the environment of high-energy hadronic interactions does not allow to trigger on the largest fraction of charm and bottom produced, the production rates are so large that the number of recorded events allows today b-physics studies that are competitive with those of e^+e^- experiments. The introduction of new experimental techniques, such as the use of silicon vertex detectors, which enable the tagging of events containing bottom quarks [3], led in the recent years to high-statistics and low-background measurements of the b-production properties over a large range of transverse momenta.

From the point of view of QCD studies, heavy-flavour production in high-energy hadronic collisions has better potentials than in fixed-target experiments. The b quarks produced at large p_T can be studied in perturbative QCD with smaller contamination from non-perturbative effects. For example, the impact of the initial-parton transverse momentum is largely reduced with respect to fixed-target charm production. Furthermore, the fragmentation properties of heavy flavours in high transverse momentum jets can be directly studied, since the transverse momenta involved are typically perturbative.

In spite of all of this, the comparison of theory with data collected by the high-energy collider experiments (UA1, CDF and D0) shows some puzzling discrepancies, which will be reviewed in the rest of this lecture. In particular, we will concentrate on the inclusive p_T distributions in the central and forward rapidity regions, and on the azimuthal correlations between b and $\bar{b}$.

3.2.1 Comparison of data and theory

The distribution most commonly studied by the hadron-collider experiments is the b-quark differential p_T spectrum, integrated within a fixed rapidity range and above a given p_T threshold (p_T^{min}):

$$\sigma(p_T^{min}) = \int_{|y|<y_{max}} d\,y \int_{p_T>p_T^{min}} d\,p_T \frac{d^2\sigma}{dy\,dp_T} \,. \tag{38}$$

The UA1 experiment at the CERN $p\bar{p}$ collider used $y_{max} = 1.5$, while the CDF and D0 experiments at the Tevatron use $y_{max} = 1$.

The results obtained by CDF [62] and D0 [63] are shown in figs. 19, compared with the theoretical predictions. For an easier evaluation of the results, we present them on a linear scale in the form Data/Theory, and include the UA1 data [64] as well. We divided the data by our central theoretical prediction. The dot-dashed straight lines are constant fits to the ratios, weighed by the inverse of the experimental uncertainties. The upper and lower solid lines correspond to the upper and lower theoretical predictions divided by the central prediction. The lower prediction is obtained fixing the renormalization and factorizations scales to be equal to $2\mu_0$ (with $\mu_0^2 \equiv {p_T}^2 + m_b^2$), and using the MRSA$'$ parton density set [65]. The value of $\Lambda_5^{\overline{\rm MS}}$ for this set (152 MeV) yields a value of α_s significantly lower than that extracted from different observables [66]. To estimate the upper theoretical curve we use the set MRS125 [31], for which $\alpha_s(M_{\rm Z}) = 0.125$, and a renormalizatoin scale equal to $\mu_0/2$. Given the large values of p_T probed by the collider experiments, the b-mass dependence of the theoretical result is small. We chose as a default the value $m_b = 4.75$ GeV, for all our curves.

The first important thing to notice in fig. 19 is that, independently of the input parameters chosen, the shape of the theoretical curves agrees well with the data. Secondly, the results at $\sqrt{S} =$ 630 GeV are by and large consistent with those at $\sqrt{S} = 1800$ GeV. The average ratio Data/Theory measured by UA1 differs by less than 10% from the ratio measured by D0, independently of the input parameters chosen. The difference is however between 40 and 50% if one uses the CDF data. If we naively average the Tevatron data, we conclude that the relative discrepancy between theory and data when changing the value of $\sqrt{S}$ from 630 to 1800 GeV is about 30%, a number of the same order of the estimate of $\log(1/x)$ effects discussed in the first lecture.

Independently of the beam energy, the data are higher by a factor of about 2 than the default prediction based on $\mu = \mu_0$. They are, however, well reproduced by the upper theoretical curve. Therefore, while the overall uncertainty of the theoretical prediction due to the scale choice is large, there is currently no serious inconsistency between theory and data for the inclusive p_T distribution of b quarks at the Tevatron. The 30% discrepancy between the results of CDF and D0 is comparable to the discrepancy between the extrapolation of the UA1 data to CDF, while UA1 and D0 data agree at the level of 10%.

Nevertheless, the discrepancy between CDF and D0 remains quite puzzling, as it is not consistent with the quoted systematic and statistical errors. In addition to this puzzle, a recent measurement of forward b production by D0 [67] (performed using muons in the rapidity range $2.4 < |\eta^\mu| < 3.2$) indicates a rate in excess by a factor of approximately 4 over the central theoretical prediction. The results are shown in fig. 20. Certainly no phenomenon of perturbative origin (such as higher-order corrections) could explain such a discrepancy.

Similar inconsistencies are found in the study of correlations. A measurement has been recently reported by CDF, using muons plus tagged b jets [68]. The shape of the $\Delta\phi$ distribution is in

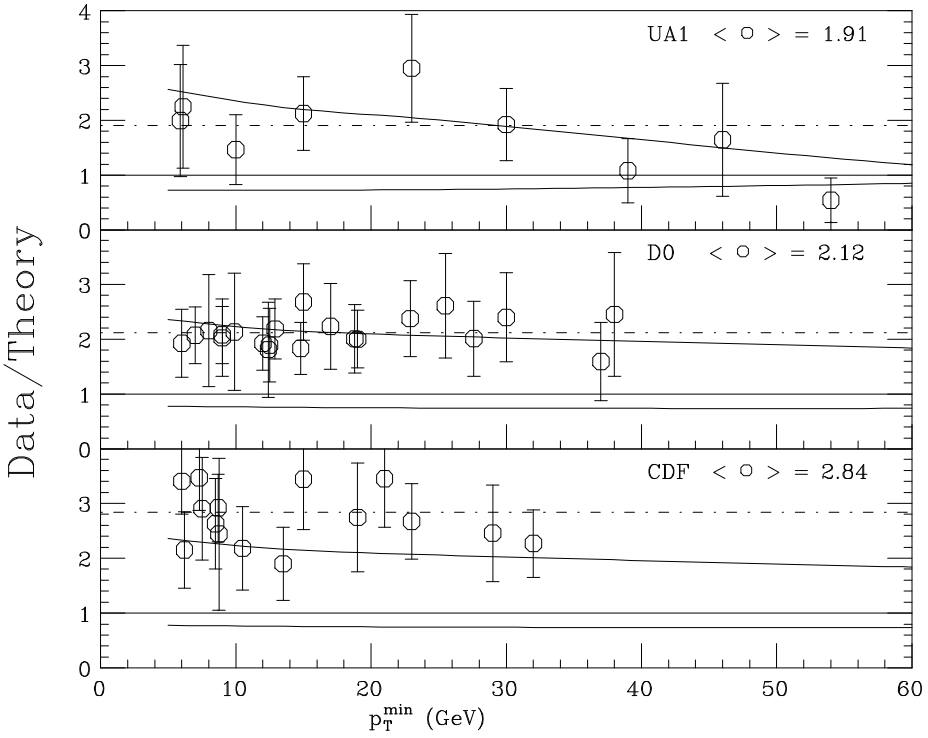

Figure 19: *Linear comparison between experimental data and theory for the integrated b-quark p_T distribution. See the text for details.*

reasonable agreement with QCD, while the distributions of the jet E_T and of the muon p_T are not (see fig. 21). On the other hand, both CDF and D0 recently presented studies based on samples of high-mass dimuons [69, 70]. The shapes for both $\Delta\phi$ and p_T^b for a given $p_T^{\bar{b}}$ are in this case well reproduced by theory, within the large uncertainties (fig. 22).

Contrary to the case of $c\bar{c}$ correlations measured in fixed-target experiments, the measurement at hadron colliders is sensitive to the modelling of the heavy-quark fragmentation, because of possible trigger biases. A harder (softer) fragmentation function would enhance (decrease) the efficiency for the detection of the softest of the two b quarks. These effects could have an impact on the distributions reported by CDF and D0. CDF explored the effects of changes in the ϵ_b parameter within the Peterson fragmentation model, finding them negligible. As we argued earlier, it cannot be excluded that a systematic study of other possible parametrizations for the fragmentation modelling could lead to significant effects. Also the possible effects of the k_T kick have been studied by CDF [68], with the conclusion that not even an average k_T as large as 4 GeV could improve the agreement between theory and data in the case of the muon plus b-tagged jet measurement.

In summary, while the overall features of b production at the Tevatron are well described by NLO QCD, there are still some apparent inconsistencies which go beyond the quoted theoretical and experimental uncertainties. I will finish these lectures by presenting some studies which have been reported recently, and others which are in progress, aimed at a better assessment of the theoretical systematics. I will first present studies related to the resummation of large perturbative logarithms, and then some considerations on the effects of non-perturbative fragmentation.

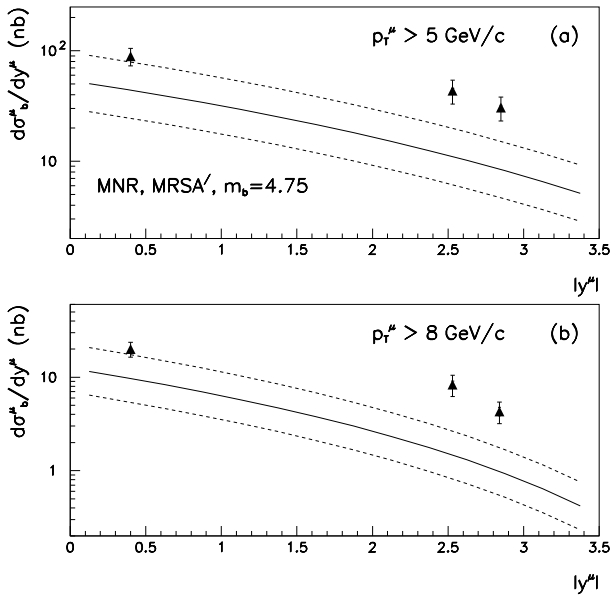

Figure 20: *Comparison between D0 data and theory for the $p\bar{p} \to (b \to \mu) + X$ cross-section at large rapidity.*

3.2.2 Resummation of large-p_T logarithms

Two different groups have approached this problem in the recent past. Cacciari and Greco [20] have folded the NLO cross-section for production of a massless parton i ($i = g, q$) [71] with the NLO fragmentation function for the transition $i \to b$ [16]. The evolution of the fragmentation functions resums all terms of order ${\alpha_s}^n \log^n(p_T/m)$ and ${\alpha_s}^{n+1} \log^n(p_T/m)$. All the dependence on the b-quark mass lies in the boundary conditions for the fragmentation functions. This approach ensures a full NLO accuracy, up to corrections of order $m^2/(m^2+p_T^2)$. In particular, this formalism describes NLO corrections to the gluon splitting process, which in the $O(\alpha_s^3)$ calculation is only included at the leading order. One can verify, by looking at the Born-level production process as a function of the quark mass, that, in order for the mass corrections not to exceed the 10% level, it is however necessary to limit the applications of this formalism to the region of $p_T \gtrsim 20$ GeV.

Figure 23 shows the differential b-quark p_T distribution obtained in the fragmentation-function approach, compared to the standard fixed-order NLO result. Several features of this figure should be noticed. To start with, the scale dependence is significantly reduced with respect to the fixed-order calculation. Furthermore, in the range of applicability of this calculation (i.e. $p_T \gtrsim 20$ GeV) the result of the fragmentation-function approach lies on the upper side of the fixed-order NLO calculation. The resummed calculation is, however, always within the uncertainty band of the fixed-order one. Finally, notice that the overall effect of the inclusion of higher-order logarithms is a steepening of the p_T spectrum, as is natural to expect.

Another calculation has recently appeared, by Scalise, Olness and Tung [21]. In this approach the authors employ a strategy developed in the case of DIS in refs. [72, 73]. Here initial- and final-state mass singularities are resummed as in the fragmentation-function approach, and the result is then matched in the low-p_T region to the fixed-order NLO massive calculation. At large p_T this

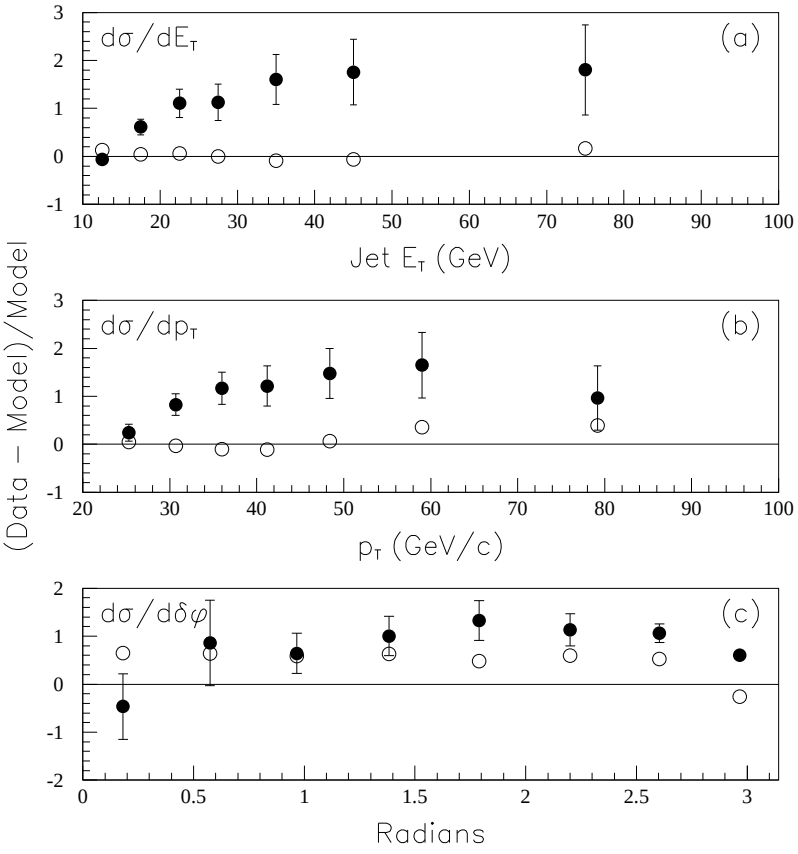

Figure 21: *CDF results on the $b\bar{b}$ correlations using μ+b-tagged jet final states [68], compared to NLO QCD. Solid points correspond to the default theoretical prediction, with scales $\mu = \mu_0$, empty circles correspond to the difference between the choice $\mu = \mu_0/2$ and $\mu = \mu_0$. Top figure: tagged-jet E_T distribution. Central: muon p_T spectrum. Bottom: azimuthal correlations.*

calculation does not include as yet, however, the full set of NLO corrections to the hard-process matrix elements.

The preliminary numerical results of this study [21] are consistent with those of the approach by Cacciari and Greco; in particular, they support the conclusion that in the p_T range explored by the Tevatron experiments the resummed results are consistent with the fixed-order ones, provided a scale μ of the order of $\mu_0/2$ or smaller is selected.

3.2.3 Non-perturbative fragmentation

We start with a remark: the use of the Peterson fragmentation function might not be justified in the context of hadroproduction of heavy quarks. As a simple observation, we point out here that while the measurement of heavy-quark spectra in e^+e^- data is mostly sensitive to the first moment of the fragmentation function, corresponding to the average jet energy carried by the heavy hadron, the p_T distributions in hadronic collisions are sensitive to higher moments of the non-perturbative fragmentation function. In fact, assuming for simplicity a perturbative p_T spectrum of the form:

$$\frac{d\sigma}{dp_T} = \frac{A}{{p_T}^n} \,, \tag{39}$$

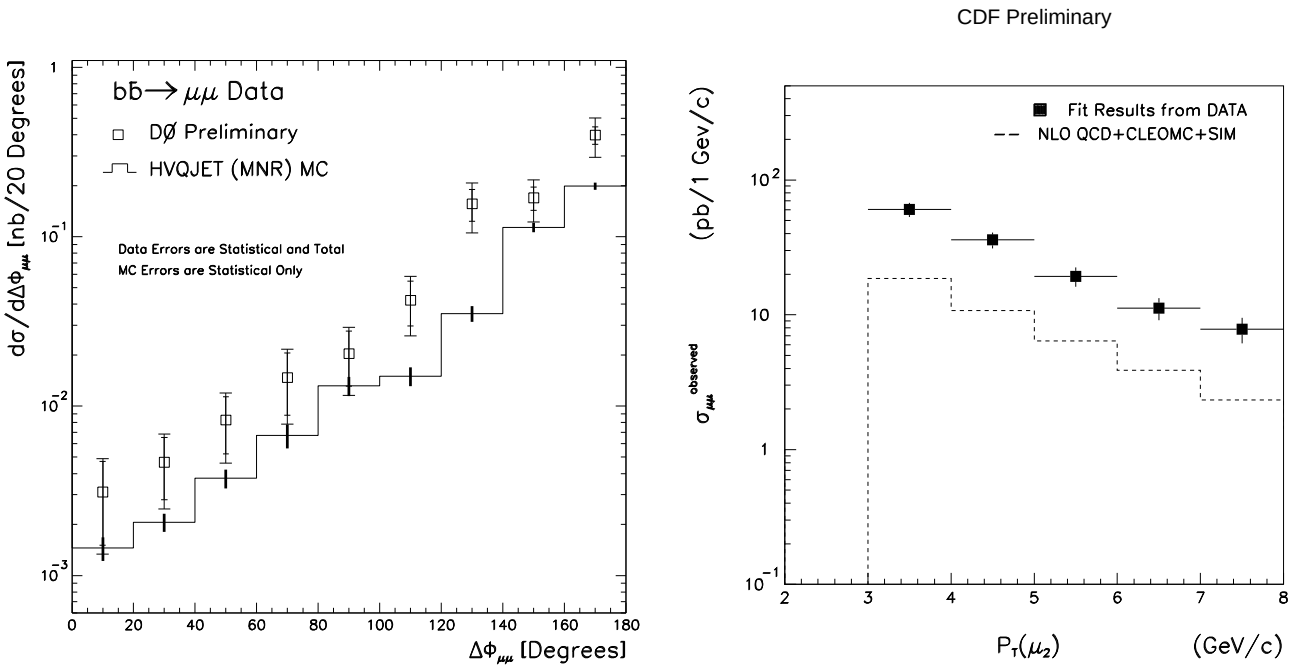

Figure 22: *Results on $b\bar{b}$ correlations using dimuon final states, compared to NLO QCD. Left: azimuthal-correlation results from D0. Right: p_T distribution of the slowest muon from CDF.*

it is easy to prove that the resulting hadron spectrum, after convolution with a given fragmentation function $f(z)$, will be given by:

$$\frac{d\sigma}{dp_T} = \frac{A}{{p_T}^n} \times \int dz\, z^{n-1}\, f(z)\ . \tag{40}$$

In the case of the Tevatron, n turns out to be approximately 5. It is not unlikely, therefore, that alternative models for the non-perturbative fragmentation of heavy quarks, which could equally well fit the e^+e^- data, could give rise to significant differences when applied to production in hadronic collisions. We also remark that the gluon component of the fragmentation function is not important in e^+e^- physics, while it may be crucial in hadroproduction.

Another important point concerns the correlation which exists between the chosen value of α_s, the accuracy at which the perturbative fragmentation function is evaluated, and the value of the parameters describing the non-perturbative fragmentation extracted from the comparison with the e^+e^- data. A larger value of α_s, and a NLO calculation, give rise to a softer perturbative fragmentation function than would be obtained from a smaller value of α_s or a LO accuracy. As a result, the non-perturbative fragmentation function will be harder. This was already noticed in the first lecture, where we compared the values of the Peterson parameter ϵ extracted from a LO and a NLO fit to the Argus and Opal D-production data ($\epsilon_c = 0.06$ at LO, $\epsilon_c = 0.01$ at NLO).

A complete study of the effect of these differences for b production at the Tevatron has not been carried out as yet. As a crude estimate of the effects, however, we can just compare the p_T spectra obtained by convoluting the fixed-order NLO calculation of the b-p_T distribution with NP fragmentation functions fitted at the LO and at the NLO. In fig. 24 I plot the ratio of the B-meson p_T distribution obtained by folding with the Colangelo-Nason fragmentation function (with the

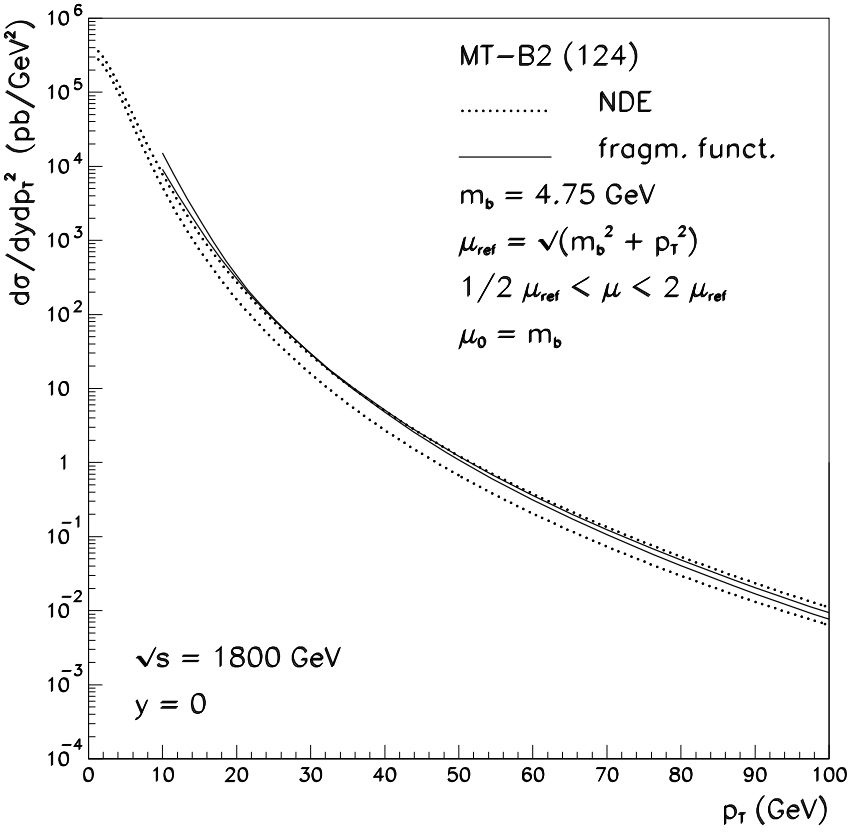

Figure 23: *Differential b-quark p_T distribution: comparison of the fixed-order NLO calculation (NDE stands for [7]) with the fragmentation-function approach [20]; μ_0 is the scale at which the boundary conditions for the fragmentation functions are set.*

parameters α and β fitted at NLO), relative to that obtained by using the Peterson fragmentation function and $\epsilon_c = 0.06$, the default choice of CDF and D0. This is done for two different rapidity intervals, one describing *central* production, the other describing *forward* production.

In the central region we obtain differences of up to 30%, which are consistent with the excess in rate reported by CDF. In the forward region the effect is larger, up to a factor of 50%, but not large enough to explain the deviation seen by D0 using their forward-muon data.

We summarize the main conclusions of the studies presented in this section:

1. There is good agreement between the shape of the b-quark p_T distribution predicted by NLO QCD and that observed in the data for central rapidities.

2. Although the data are higher by a factor of approximately 2 with respect to the theoretical prediction with the default choice of parameters, extreme (although acceptable) choices of $\Lambda_5^{\overline{\rm MS}}$ and of renormalization and factorization scales bring the theory in perfect agreement with the data of UA1 and D0, and within 30% of the CDF measurements.

3. The choice of low values of $\mu_{\rm R}$ and $\mu_{\rm F}$, which helps the agreement between theory and data, is favoured by studies of higher-order logarithmic corrections.

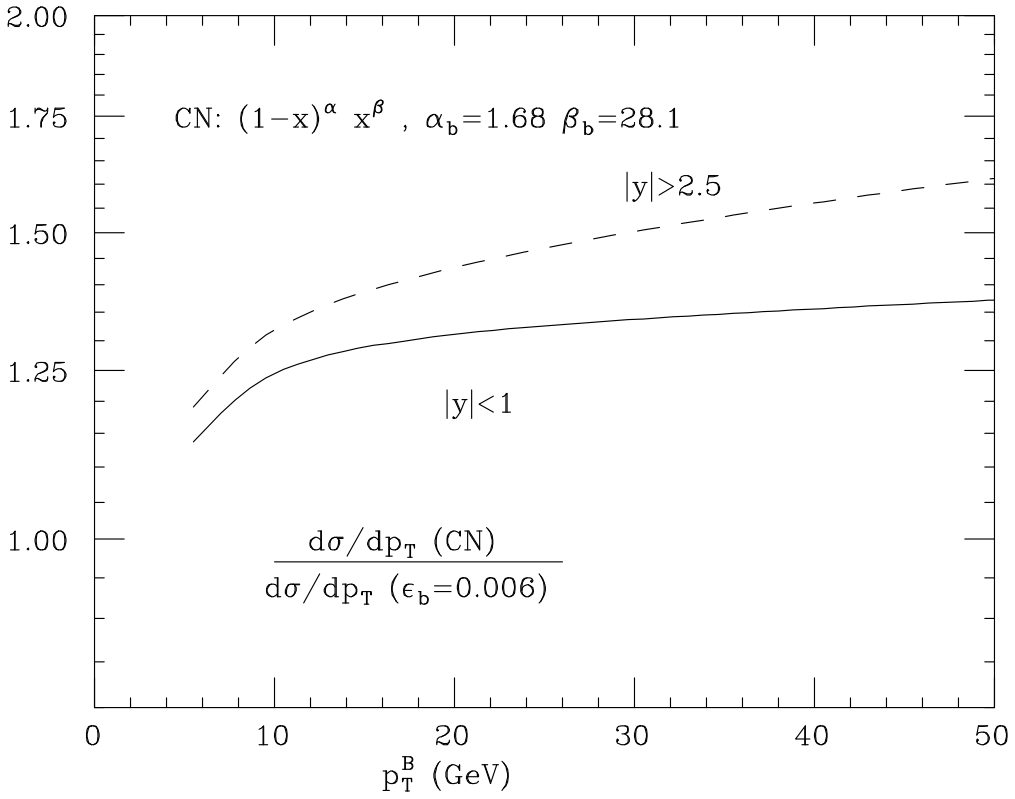

Figure 24: *Ratio of the B-meson p_T distribution using the Colangelo-Nason fragmentation function (with the parameters α and β fitted at NLO), relative to that obtained by using the Peterson fragmentation function and $\epsilon_c = 0.06$. Central production (solid) and forward production (dashes).*

4. The 30% difference between CDF and D0 cannot be explained by theory, and will need to be understood before further progress can be made.

5. Forward production of b quarks at D0 indicates a larger discrepancy between theory and data, which cannot be accomodated by higher-order perturbative corrections, nor by the systematic uncertainties induced by the choice of non-perturbative fragmentation functions.

As should be clear from the list above, more work is necessary both on the experimental and on the theoretical sides to improve our understanding of bottom production at high energy. To which extent the current inconsistencies will affect future physics plans at the Tevatron and at the LHC it is not clear. It is unlikely however that measurements such as CP asymmetries will be affected by these issues, since they rely on ratios of rates. Nevertheless the study of b production remains an important test of our ability to perform solid perturbative predictions, and any progress which can be made in the coming future will certainly benefit our understanding of QCD at high energies.

Acknowledgements: I am very grateful to L. Moroni and I. Bigi for the invitation to attend this School. I also wish to thank my collaborators, S. Frixione, P. Nason and G. Ridolfi, with whom most of the work presented here was done over the years.

References

[1] F. Abe et al., CDF Coll., *Phys. Rev.* **D50**(1994)2966;
S. Abachi et al., D0 Collaboration, *Phys. Rev. Lett.* **79**(1997)1197;
F. Abe et al., CDF Collaboration, FERMILAB-PUB-97-284-E.

[2] J.H. Kuehn, Lectures delivered at 23rd SLAC Summer Institute, Stanford, CA, 10-21 Jul 1995, `hep-ph/9707321;`
Y. Sumino, *Acta Phys.Polon.* **B25**(1994)1837.

[3] F. Bedeschi, Lectures at this School.

[4] S. Stone, Lectures at this School. `hep-ph/9709500.`

[5] P. Nason, "Heavy Quark Production", in "Heavy Flavours", eds. J. Buras and M. Lindner, Advanced Series on Directions in High Energy Physics, World Scientific Publishing Co.

[6] R.K. Ellis, W.J. Stirling and B.R. Webber, *QCD and Collider Physics*, Cambridge University Press (1996).

[7] P. Nason, S. Dawson and R. K. Ellis, *Nucl. Phys.* **B303**(1988)607.

[8] W. Beenakker, H. Kuijf, W.L. van Neerven and J. Smith, *Phys. Rev.* **D40**(1989)54.

[9] P. Nason, S. Dawson and R. K. Ellis, *Nucl. Phys.* **B327**(1989)49, erratum *ibid.* **B335**(1990)260.

[10] W. Beenakker, W. L. van Neerven, R. Meng, G. A. Schuler and J. Smith, *Nucl. Phys.* **B351**(1991)507.

[11] R. K. Ellis and P. Nason, *Nucl. Phys.* **B312**(1989)551.

[12] J. Smith and W.L. van Neerven, *Nucl. Phys.* **B374**(1992)36.

[13] M.L. Mangano, P. Nason and G. Ridolfi, *Nucl. Phys.* **B373**(1992)295.

[14] S. Frixione, M.L. Mangano, P. Nason and G. Ridolfi, *Nucl. Phys.* **B412**(1994)225.

[15] Ya.I. Azimov, Yu.L. Dokshitser, V.A. Khoze, *Sov.J.Nucl.Phys.* **36**(1982)878.

[16] B. Mele and P. Nason, *Nucl. Phys.* **B361**(1991)626.

[17] S. Catani, M. Ciafaloni and F. Hautmann, *Nucl. Phys.* **B366**(1991)135.
[18] J. C. Collins and R. K. Ellis, *Nucl. Phys.* **B360**(1991)3.
[19] J.C. Collins and Wu-Ki Tung, *Nucl. Phys.* **B278**(1986)934.
[20] M. Cacciari and M. Greco, *Nucl. Phys.* **B421**(1994)530, `hep-ph/9311260`.
[21] R.J. Scalise, F.I. Olness and W.-K. Tung, SMU-HEP-96-08.
[22] C. Peterson, D. Schlatter, I. Schmitt and P. Zerwas, *Phys. Rev.* **D27**(1983)105.
[23] G. Colangelo and P. Nason, *Phys. Lett.* **B285**(1992)177.
[24] H. Albrecht et al., ARGUS coll., *Z. Phys.* **C52**(1991)353.
[25] R. Akers et al., OPAL Coll., *Z. Phys.* **C67**(1995)27.
[26] M. Cacciari and M. Greco, *Phys. Rev.* **D55**(1997)7134.
[27] J. Chrin, *Z. Phys.* **C36**(1987)163.
[28] G. Alexander et al., OPAL Coll., *Phys. Lett.* **B369**(1996)163.
[29] S. Frixione, M.L. Mangano, P. Nason and G. Ridolfi, to be published in Heavy Flavours II, ed. by A.J. Buras and M. Lindner, World Scientific, `hep-ph/9702287`.
[30] E.M. Aitala et al., E791 Coll., *Phys. Lett.* **B371**(1996)157.
[31] A.D. Martin, R.G. Roberts and W.J. Stirling, *Phys. Lett.* **B356**(1995)89, `hep-ph/9506423.`
[32] P.J. Sutton, A.D. Martin, R.G. Roberts and W.J. Stirling, *Phys. Rev.* **D45**(1992)2349.
[33] M. Aguilar-Benitez et al., LEBC-EHS Coll., *Phys. Lett.* **B161**(1985)400; S. Barlag et al., ACCMOR Coll., *Z. Phys.* **C39**(1988)451; S. Barlag et al., ACCMOR Coll., *Z. Phys.* **C49**(1991)555; K. Kodama et al., E653 Coll., *Phys. Lett.* **B284**(1992)461.
[34] G.A. Alves et al., E769 Coll., *Phys. Rev. Lett.* **77**(1996)2388.
[35] M.I. Adamovich et al., WA92 Coll., *Nucl. Phys.* **B495**(1997)3.
[36] K. Kodama et al., E653 Coll., *Phys. Lett.* **B263**(1991)573.
[37] R. Ammar et al., LEBC-MPS Coll., *Phys. Rev. Lett.* **61**(1988)2185.
[38] M. Aguilar-Benitez et al., LEBC-EHS Coll., *Z. Phys.* **C40**(1988)321.
[39] G. Bari et al., *Nuovo Cimento* **104A**(1991)1787. M. Basile et al., *Nuovo Cimento* **65A**(1981)391; K. Kodama et al., E653 Coll., *Phys. Lett.* **B303**(1993)359; M.G. Catanesi et al., WA78 Coll., *Phys. Lett.* **231B**(1989)328; P. Bordalo et al., NA10 Coll., *Z. Phys.* **C39**(1988)7; R. Jesik et al., E672-E706 Coll., *Phys. Rev. Lett.* **74**(1995)495.
[40] D.M. Jansen et al., E789 Coll., *Phys. Rev. Lett.* **74**(1995)3118.
[41] T. Alexopoulos et al., E771 Collaboration, FERMILAB-PUB-97-246-E.
[42] M.P. Alvarez et al., NA14/2 Coll., *Z. Phys.* **C60**(1993)53.
[43] J.C. Anjos et al., E691 Coll., *Phys. Rev. Lett.* **62**(1989)513.
[44] J.C. Anjos et al., E691 Coll., *Phys. Rev. Lett.* **65**(1990)2503.
[45] G. Bellini, Proc. of Les Rencontres de Physique de la Vallée d'Aoste, La Thuile, 1994.
[46] S. Aoki et al., WA75 Coll., *Phys. Lett.* **B209**(1988)113.
[47] G.A. Alves et al., E769 Coll., *Phys. Rev. Lett.* **69**(1992)3147.
[48] M.I. Adamovich et al., WA82 Coll., *Nucl. Phys. (Proc. Suppl.)* **B27**(1992)212.
[49] S. Aoki et al., WA75 Coll., *Progr. Theor. Phys.* **87**(1992)1315, erratum *ibid.* **88**(1992)621; *Phys. Lett.* **B209**(1988)113.
[50] G.A. Alves et al., E769 Coll., *Phys. Rev. Lett.* **77**(1996)2392.
[51] L. Apanasevich et al., E706 Coll., *Phys. Rev.* **D56**(1997)1391.
[52] M. Aguilar-Benitez et al., LEBC-EHS Coll., *Phys. Lett.* **B164**(1985)404.
[53] M.I. Adamovich et al., Photon Emulsion Coll., *Phys. Lett.* **B187**(1987)437 and references therein.

[54] S. Barlag et al., ACCMOR Coll., *Phys. Lett.* **B257**(1991)519.
[55] K. Kodama et al., E653 Coll., *Phys. Lett.* **B263**(1991)579.
[56] M.P. Alvarez et al., NA14/2 Coll., *Phys. Lett.* **B278**(1992)385.
[57] P. Frabetti et al., E687 Coll., *Phys. Lett.* **B308**(1993)193.
[58] M.I. Adamovich et al., WA92 Coll., *Phys. Lett.* **B385**(1996)487.
[59] M.L. Mangano, P. Nason and G. Ridolfi, *Nucl. Phys.* **B405**(1993)507.
[60] S. Frixione, M.L. Mangano, P. Nason and G. Ridolfi, *Nucl. Phys.* **B431**(1994)453.
[61] M.I. Adamovich et al., WA92 Coll., *Phys. Lett.* **B348**(1995)256.
[62] F. Abe et al., CDF Coll., *Phys. Rev. Lett.* **68**(1992)1104; *ibid.* **69**(1992)3704; *ibid.* **71**(1993)500; *ibid.* **71**(1993)2396; *ibid.* **71**(1993)2537.
[63] S. Abachi et al., D0 Coll., *Phys. Rev. Lett.* **74**(1995)3548; *Phys. Lett.* **B370**(1996)239.
[64] C. Albajar et al., UA1 Coll., *Phys. Lett.* **B256**(1991)121, erratum *ibid.* **B262**(1991)497.
[65] A.D. Martin, R.G. Roberts and W.J. Stirling, *Phys. Lett.* **B354**(1995)155.
[66] Particle Data Group, R.M. Barnett et al., *Phys. Rev.* **D54**(1996)1.
[67] S. Abachi et al., D0 Coll., submitted to the Int. Conf. on High Energy Physics, Warsaw, 1996, paper Pa05-025.
[68] F. Abe et al., CDF Coll., *Phys. Rev.* **D53**(1996)1051, `hep-ex/9508017.`
[69] F. Abe et al., CDF Coll., *Phys. Rev.* **D55**(1997)2546.
[70] S. Abachi et al., D0 Coll., submitted to the Int. Conf. on High Energy Physics, Warsaw, 1996, paper Pa05-023.
[71] F. Aversa, P. Chiappetta, M. Greco and J.P. Guillet, *Nucl. Phys.* **B327**(1989)105.
[72] M.A.G. Aivazis, F.I. Olness and Wu-Ki Tung, *Phys. Rev.* **D50**(1994)3085, `hep-ph/9312318.`
[73] M.A.G. Aivazis, J.C. Collins, F.I. Olness and Wu-Ki Tung, *Phys. Rev.* **D50**(1994)3102, `hep-ph/9312319.`